1-1-2013

Modeling Volume Change Due to Intercalation Into Porous Electrodes

Kumud Kanneganti
University of South Carolina

Modeling volume change due to intercalation into porous electrodes

by

Kumud Kanneganti

Bachelor of Technology
Nirma Institute of Technology, 2008

Master of Science
New Jersey Institute of Technology, 2010

Submitted in Partial Fulfillments of the Requirements

For the Degree of Master of Science in

Chemical Engineering

College of Engineering and Computing

University of South Carolina

2013

Accepted by:

John W. Weidner, Major Professor

Xinyu Huang, Committee Member

Edward P. Gatzke, Committee Member

Lacy Ford, Vice Provost and Dean of Graduate Studies

DEDICATION

To my loving parents Swaroopa and Sudhakar Kanneganti

and to the love of my life Anshika

ACKNOWLEDGMENT

I would like to take this opportunity to express my gratitude towards my advisor Dr. John Weidner, Professor and Chair of the Department of Chemical Engineering, University of South Carolina for providing me with an opportunity to work with him. This not only gave me immense pleasure but also provided me with a platform to grow. I would like to thank him for his guidance and invaluable advice throughout the course of this study.

I am also thankful to my co-advisor, Dr. Xinyu Huang, Assistant Professor, Department of Mechanical Engineering, University of South Carolina for his timely advice and valuable inputs without which this project would have been impossible. I would also like to thank my committee member, Dr. Edward Gatzke, Associate Professor, Department of Chemical Engineering, University of South Carolina for agreeing to be on the committee. I would also like to thank Dr. Javid Moraveji for his guidance and Dr. Long Cai for his timely help and lastly I would like to thank my family and friends for the unconditional love and support they have given me throughout my endeavors.

ABSTRACT

Electrochemical devices (batteries, fuel cell) are expected to play a vital role in the future of energy consumption for various purposes ranging from house hold usage to space exploration. Research is being conducted on various aspects so as to improve the design and operating range of these devices and one of the primary focuses is the porous electrode. It has been reported that significant volume change can occur during electrode processes, within the porous electrodes and depending on the material it can be as high as, but not limited to 300%. These large volume changes along with product formation in pores can cause severe mechanical and performance degradation. However, prediction of stresses generated inside the electrode is highly empirical. Predictive models could give crucial insight into design parameters. Here we have formulated a continuum presentation of the porous material which combines mechanics of the solid phase of the porous material with the dependence of porosity on stress, as in rock-mechanics. In this new model, the deformation of the porous electrode material is characterized by its compressibility. Using the analogy between thermal stress-strain relationships and stress-strain relationship for existing concentration gradients, a constitutive law for the volumetric strain of the electrode during intercalation is developed, facilitating the prediction of volume and porosity change from fundamental material properties. The model is general and in conjunction with appropriate boundary and initial conditions, can be used to predict the volume and porosity change of any electrode during operation.

TABLE OF CONTENTS

LIST OF FIGURES

LIST OF SYMBOLS

A	Cross-sectional area of porous electrode, cm^2
C	Compressibility, 1/Pa
E	Cell Potential, V
$\mathcal{F}$	Faraday's constant, 96487 C/mol
g	Swelling coefficient
g_x	Splitting parameters introduced in Eq. [30]
g_y	Splitting parameters introduced in Eq. [30]
g_z	Splitting parameters introduced in Eq. [30]
I	Total applied current, A
j	Local volumetric electrochemical reaction rate, A/cm^3
n	Number of electron transfers in electrochemical reaction
R_i	Ionic resistance of porous electrode, Ω
s	Stoichiometric coefficient of the product in electrochemical reaction

t	Time, s
$\boldsymbol{u}$	Local velocity vector in the electrode, m/s
$\boldsymbol{u}_x$	Local velocity component in the vector in x direction, m/s
$\boldsymbol{u}_y$	Local velocity component in the vector in y direction, m/s
$\boldsymbol{u}_z$	Local velocity component in the vector in z direction, m/s
V	Total electrode volume, m^3
$\Delta\hat{V}$	Change in molar volume of reaction product, m^3/mol
x	Sate of Charge
Q	Charge carried by the electrode, C

Greek

ε	Porosity
φ	Volumetric strain
φ_x	Strain of the dimension in x direction
φ_y	Strain of the dimension in y direction
φ_z	Strain of the dimension in z direction
σ	Hydrostatic stress, Pa

$\hat{\sigma}$	Dimensionless stress, $C_c\sigma$
θ	Relative compressibility

Superscript

0	Initial
max	Maximum

Subscript

C	Casing
E	Electrode
I	Intercalation
M	Mechanical

Chapter 1: INTRODUCTION

Portable lithium ion batteries (LIB) make up about 63% of the worldwide sales. Due to this there is a constant demand for developing more compact and higher energy density batteries. A multidisciplinary study of new material can help understand and develop better electrode material [1], which can then be used in developing devices with better functionality [2]. Rechargeable batteries generally make use of porous electrodes that provide very high surface areas in a compact dimension, which simultaneously reduces ohmic, mass transfer and kinetic losses [3]. The electrode is essentially an aggregate of active particles which are generally fabricated using micro and nanofabrication technologies to get ordered arrays of the active material [4, 5]. Rechargeable batteries are built for continuous use, which implies they undergo frequent charge/discharge cycles. Each charge/discharge cycle consists of ions moving from one electrode to the other and back. This movement of ions from/into the active material causes volume changes and these frequent volume changes may lead to cracking and/or delamination of the active material [6-11] either from the binder and/or itself. Advanced electrode material like Tin and Silicon have higher energy density but also undergo volume change of about 300% during cycling [12]. For this reason it becomes imperative to study various parameters that affect the age of the electrode. Mechanical degradation by fracture and delamination of the electrode particles results in loss of contact of active material and creation of new surfaces exposed to the electrolyte which may cause the formation of a new solid

electrolyte interface. To understand and accurately predict the behavior of electrochemical devices (e.g., fuel cell), it is necessary to develop sophisticated computer models that incorporate the complex interactions of electrochemical performance (e.g., current-voltage relationship), mechanical strength, structural deformations and operating life. Among them, the change in volume of the electrode is important as it plays an important role in generation of stresses [13]. Most research to date is focused on predicting the electrochemical performance of these devices [14-23]. Predicting the mechanical stresses of porous electrodes based on the volume changes in solid-electrode material, which has not been done before, is the focus of this work.

Porous electrodes are inherently different from plain electrodes because of close contact between the solid phase (matrix) and the electrolyte due to this it is impossible to separate mass transfer and electrode processes. Hence to model the operation of porous electrodes, porous electrode theory is used. Average of various variables over a region of the electrode small with respect to the overall dimensions but large compared to the pore dimensions are considered [24]. The quantities defined herein are assumed to be a continuous function of the time and space coordinates. Since the quantities are averaged, it allows the treatment of the volume element in the porous electrode as a fraction of solid volume and a fraction of liquid volume, essentially converting the complex 3-D problem into a 1-D problem.

Early attempts to predict volume change in the porous electrodes considered that only porosity was affected. For example, Alkire et al. [25] developed a model for describing the non-uniform porosity changes with constant electrode volume and Dunning et al. [26]

developed a model for describing the effects of changing porosity and reaction surface area in addition to charge and mass-transport occurring in the electrodes.

To account for variation in the active material, without abandoning the advantage of the averaged quantities in the porous electrode theory, pseudo 2-D models were developed. These models defined the electrode microstructure using simplified geometries, for example spherical geometries and integrated this with the existing porous electrode theory. For example, Fuller et al. [27] developed a general model assuming for dual lithium ion insertion cells to discuss the importance of diffusion of lithium into the solid phase meanwhile, Doyle et al. [28] developed a general battery model with graphite and lithium-manganese spinel electrodes to predict diffusion inside the electrodes. Pseudo 2-D models are able to capture more details regarding the porous electrode as compared to the models developed using porous electrode theory

Jain et al. [29, 30] and Cai et al. [31], both authors developed models to account for only the change in porosity of the electrode whereas the dimensions of the electrode were assumed to be constant. It is found that experimentally when an insertion electrode undergoes volume expansion, there is a change in dimensions and change in porosity. Gomadam et al. [32] developed a mathematical model to describe volume change in porous electrodes in all three dimensions by accounting for the change in the dimensions of the electrode and the change in porosity of the electrode. During the model development, a constant design parameter called the swelling coefficient is defined which enables the determination of the fraction of volume expansion that goes towards the change in dimensions of the electrode and the fraction of volume expansion that changes the

porosity of the electrode during operation. This parameter was approximated as it was dependent on the stresses generated inside the porous electrode.

Several authors later developed Single Particle (SP) models to study stress generation during volume change in a single particle, insertion material, with diffusion inside the particle. Since there is no information available on how individual particles interact with each other, these models cannot be extended to the entire electrode. Using spherical geometries, Christensen and Newman [14, 18] developed a model to show the evolution of Diffusion Induced Stress (DIS) with the volume change of the particle due to non-uniform reaction rates. Zhang et al. [19, 33] studied DIS and heat generation for volume change in a $LiMn_2O_4$ spherical and ellipsoidal cathode particle, whereas Park et al. [20] studied DIS due to phase transition in $LiMn_2O_4$ particles, to conclude that there is higher stress generation due to phase change. Some authors even performed fracture analysis, like Deshpande et al. [34], who examined DIS developed at the phase boundary of the particle using strain energy as criteria for crack propagation. Eventually SP models were also developed to look at different geometries like cylindrical [35, 36], hollow sphere [37], hollow cylinder [38] and some unique geometries [39]. Some authors used these SP models and integrated it with porous electrode theory to develop pseudo 2-D models, like Renganathan et al. [40] who studied the effects of design parameters like effective thickness and porosity on cell potential and Cai et al. [31].

In this work, a model is developed to predict stresses in the entire porous electrode, by using formulations in rock mechanics. The deformation of the porous rock during the application of stress is characterized by its compressibility [41] is combined with stress-strain relationship for existing concentration gradients [33], to obtain a constitutive law for

the volumetric strain of the electrode during intercalation. The compressibility data of the electrode has to be obtained experimentally, for this work compressibility is suitably approximated. Using this newly developed stress-strain relationship, the change in porosity during intercalation can also be predicted. The prediction of fractions of volume expansion being directed towards dimensional change and porosity change is also possible. The above model is general and in conjunction with appropriate boundary and initial conditions, it can be used to predict the volume change of any electrode.

Chapter 2: MODEL DEVELOPMENT

During operation, the intercalation electrode undergoes frequent volume changes due to the insertion/de-insertion of intercalates (product of the electrochemical reaction) into/from the active material, generating stresses which may lead to mechanical failures like delamination or pulverization of the electrode. The active material of only one electrode, when expanding fills out part of the pore volume and simultaneously generates stresses due to mechanical constraints, on the other hand when the electrode is shrinking, it generates pore volume and simultaneously relaxes from a pre-stressed state. The material balance over the solid phase (active material + reaction product) governs the volume change as,

$$\frac{\partial}{\partial t}(1-\varepsilon) + \mathbf{u}\cdot\boldsymbol{\nabla}(1-\varepsilon) + (1-\varepsilon)\boldsymbol{\nabla}\cdot\boldsymbol{u} = -\frac{s\,\Delta\widehat{V}}{n\mathcal{F}}j \qquad [1]$$

For the definition of the above used variables, look at the List of Symbols. Here, the porosity, the local electrode velocity and the local volumetric current density are assumed to be a continuous function of location. The local electrode velocity is a smooth function thus its gradient can further be expressed as rate change of the volumetric strain,

$$\boldsymbol{\nabla}\cdot\boldsymbol{u} = \frac{\partial}{\partial x_i}\frac{\partial}{\partial t}\boldsymbol{u_i} = \frac{\partial}{\partial t}\frac{\partial}{\partial x_i}\boldsymbol{u_i} = \frac{\partial}{\partial t}\boldsymbol{u_{i,i}} = \frac{\partial}{\partial t}\left[\frac{1}{2}\left(\boldsymbol{u_{i,i}} + \boldsymbol{u_{i,i}}\right)\right] = \frac{\partial\varphi}{\partial t} \qquad [2]$$

Using Eq. [2] in Eq. [1] gives the governing relationship between the porosity and the volumetric strain of the electrode during intercalation.

$$\frac{\partial}{\partial t}(1-\varepsilon) + \boldsymbol{u}\cdot\boldsymbol{\nabla}(1-\varepsilon) + (1-\varepsilon)\frac{\partial \varphi}{\partial t} = -\frac{s\,\Delta\hat{V}}{n\mathcal{F}}j \quad [3]$$

Assuming uniform porosity distribution (i.e. ε is uniform), Eq. [3] can be simplified as

$$\frac{\partial}{\partial t}(1-\varepsilon) + (1-\varepsilon)\frac{\partial \varphi}{\partial t} = -\frac{s\,\Delta\hat{V}}{n\mathcal{F}}j \quad [4]$$

The volumetric strain of the electrode, analogous to thermal-mechanical strain [33] is made up of two parts. The first is the mechanical strain, 'φ_{M}' (caused by the mechanical stress) and the second is the intercalation strain, 'φ_{I}' (caused by the addition of intercalate into the solid phase). Mathematically the volumetric electrode strain can be expressed as

$$\varphi = \varphi_M + \varphi_I \quad [5]$$

Considering uniform expansion everywhere in the electrode, i.e. assuming that there are no transport limitations within the active material of the electrode, and also since the volume of the porous material can be measured before and after intercalation. The intercalation strain of the electrode can be defined similar to Obrovac et al. [13] as,

$$\varphi_I = \left[\frac{\Delta\hat{V}}{\hat{V}^0}\right]x \quad [6]$$

For a porous electrode treated as a continuum of fractions of solid phase and pores, the compressibility analogous to the treatment in rock mechanics [41, 42] is defined as,

$$C_E = -\frac{1}{V}\frac{dV}{d\sigma} \quad [7]$$

The mechanical volume of the electrode is defined as

$$V_M = V^0(1+\varphi_M) \quad [8]$$

Differentiating Eq. [8] and noting that mechanical stress (σ) only affects the volume change due to mechanical strain, the relative volume change can be re-written as

$$\frac{dV_M}{V_M} = \frac{d(1+\varphi_M)}{(1+\varphi_M)} \quad [9]$$

Substitution of Eq. [9] into Eq. [7] and performing integration gives the mechanical strain of the electrode as

$$\varphi_M = exp(-C_E\sigma) - 1 \quad [10]$$

The total electrode strain is then defined by using Eq. [5], Eq. [6] and Eq. [10] as,

$$\varphi = exp(-C_E\sigma) - 1 + \left[\frac{\Delta\hat{V}}{\hat{V}^0}\right] x \quad [11]$$

Typically the porous electrodes are enclosed in a casing to hold the electrolyte, provide support to the electrodes and facilitate electrical contact. A casing restrains volume expansion of the electrodes and hence induces mechanical stresses within the electrode. It is assumed that the casing undergoes small to medium deformation when there is large deformation in the electrode. Due to this the total electrode strain (battery strain) is given as

$$\varphi = \sigma C_C \quad [12]$$

Here C_C is an equivalent compressibility of casing. It represents the ratio of incremental volume strain of the casing to incremental internal pressure inside the casing. A linear relationship is assumed here. Eq. [11] in dimensionless form, in given as,

$$\varphi = exp(-\theta\hat{\sigma}) - 1 + \left[\frac{\Delta\hat{V}}{\hat{V}^0}\right] x \quad [13]$$

Here, $\hat{\sigma}$ is the dimensionless stress given as the product of stress and the compressibility of the casing and θ, is defined as the ratio of electrode to casing compressibility, given as

$$\theta = \frac{C_E}{C_C} \quad [14]$$

Eq. [12], the strain of the casing in dimensionless form is,

$$\varphi = \hat{\sigma} \quad [15]$$

Using Eq. [5] and Eq. [12], the derivative of the total electrode strain is written as

$$\frac{d\varphi}{dt} = \frac{d\varphi_M(\sigma)}{dt} + \frac{d\varphi_I}{dt} = C_C \frac{d\sigma}{dt} \quad [16]$$

Since mechanical strain is only a function of stress, Eq. [16] can be re-written as

$$\frac{d\varphi_M(\sigma)}{d\sigma}\frac{d\sigma}{dt} + \frac{d\varphi_I}{dt} = C_C \frac{d\sigma}{dt} \quad [17]$$

The porosity can be defined as a function of only stress, similar to the treatment in rock mechanics [41 – 43]. Using Eq. [17], Eq. [4] can be rewritten as

$$\frac{\partial}{\partial\sigma}(1-\varepsilon) + (1-\varepsilon)C_{\mathrm{C}} = -\frac{s\,\Delta\hat{V}}{n\mathcal{F}} j \left(\frac{C_{\mathrm{c}} - \frac{d\varphi_M}{d\sigma}}{\frac{d\varphi_I}{dt}}\right) \quad [18]$$

Differentiating Eq. [10] with respect to stress (σ) and Eq. [6] with respect to time (t) and then using them in Eq. [18] gives:

$$\frac{d}{d\sigma}(1-\varepsilon) + (1-\varepsilon)C_c = -\frac{s\,\hat{V}^0}{n\mathcal{F}} j\, C_c \left[1 + \frac{C_E}{C_c} exp(-C_E\sigma)\right]\frac{dt}{dx} \quad [19]$$

For illustrative purposes we assume uniform reaction current (I) i.e.

$$j = \frac{I}{V} \quad [20]$$

The volume of the electrode is defined as

$$V = V^0(1+\varphi) \quad [21]$$

Using Eq. [20] and Eq. [21] in Eq. [19] gives

$$\frac{d}{d\sigma}(1-\varepsilon) + (1-\varepsilon)C_c = C_c(1-\varepsilon^0)\frac{[1+\theta exp(-C_E\sigma)]}{[1+\sigma C_c]} \quad [22]$$

The electrode porosity-stress relationship given by Eq. [22] can be rewritten in dimensionless form as

$$\frac{d}{d\hat{\sigma}}(1-\varepsilon) + (1-\varepsilon) = (1-\varepsilon^0)\frac{[1+\theta exp(-\theta\hat{\sigma})]}{[1+\hat{\sigma}]} \quad [23]$$

Performing integration on Eq. [22] gives the porosity of the electrode as a function of stress

$$\varepsilon(\sigma) = 1 - (1-\varepsilon^0)e^{(-1-\sigma C_c)}\mathrm{Ei}(1,-1-\sigma C_c) - \theta(1-\varepsilon^0)\, e^{(-1+\theta\,-\sigma C_c)}\mathrm{Ei}(1,-1+\theta+(-1+\theta\,)\sigma C_c) \; + \; ce^{(-\sigma C_c)} \quad [24]$$

Here, Ei is the exponential integral function, it is defined as [44]

$$\mathrm{Ei}(x) = \int_x^\infty e^{-t}/t\, dt \quad \text{for } x > 0 \quad [25]$$

The discussion in Gomadam et al.[32] defined a constant parameter called as the swelling coefficient which determines the fraction of volume expansion that goes into the change in porosity and the fraction that goes into the change in dimensions of the electrode (volume of the electrode) and is defined as

$$g = \frac{\frac{d\,lnV}{d\,ln(1-\varepsilon)}}{1+\frac{d\,lnV}{d\,ln(1-\varepsilon)}} \quad [26]$$

In this paper, the swelling coefficient is not held constant as in Gomadam et al. [32] but is calculated similarly during intercalation. Using Eq. [11] and Eq. [12] in Eq. [26], the analytical solution for the swelling coefficient is given as,

$$g = \frac{(1-\varepsilon)}{(1-\varepsilon^0)[1+\theta exp(-C_E\sigma)\,]-(1-\varepsilon)C_C\sigma} \quad [27]$$

During the expansion of the porous electrodes, there is change in dimensions of the electrode, which may or may not be uniform. To calculate the change in dimensions of the electrode, it is then necessary to calculate the individual components of the velocity. Substituting Eq. [16] and using Eq. [17] in Eq. [2] we can write

$$\boldsymbol{\nabla}\cdot\boldsymbol{u} = \frac{d\varphi}{dt} = C_c\frac{\frac{d\varphi_I}{dt}}{C_c-\frac{d\varphi_M}{d\sigma}} \quad [28]$$

When the local electrode velocity is expressed as individual components, Eq. [28] is re-written as

$$\frac{d\boldsymbol{u}_x}{dx}+\frac{d\boldsymbol{u}_y}{dy}+\frac{d\boldsymbol{u}_z}{dz} = \frac{d\varphi}{dt} = \left[\frac{\Delta\widehat{V}}{\widehat{V}^0}\right]\frac{dx}{dt}\left(\frac{1}{1+\theta exp(-C_E\sigma)}\right) \quad [29]$$

To obtain local electrode velocities in each direction, Eq. [28] can be spilt by introducing splitting parameters g_x, g_y and g_z to give,

$$\frac{d\boldsymbol{u}_x}{dx} = g_x\left[\left[\frac{\Delta\widehat{V}}{\widehat{V}^0}\right]\frac{dx}{dt}\left(\frac{1}{1+\theta exp(-C_E\sigma)}\right)\right] \quad [30a]$$

$$\frac{d\boldsymbol{u}_y}{dx} = g_y\left[\left[\frac{\Delta\widehat{V}}{\widehat{V}^0}\right]\frac{dx}{dt}\left(\frac{1}{1+\theta exp(-C_E\sigma)}\right)\right] \quad [30b]$$

$$\frac{d\boldsymbol{u}_z}{dx} = g_z \left[\left[\frac{\Delta \hat{V}}{\hat{V}^0} \right] \frac{dx}{dt} \left(\frac{1}{1 + \theta exp(-C_E \sigma)} \right) \right] \quad [30c]$$

Here the splitting parameters g_x, g_y and g_z, determine how much of the electrode's dimensional change is due to the change in the dimensions in x, y and z direction. They can be defined as, similar to Gomadam et al. [40]

$$g_x = \frac{d\varphi_x}{d\varphi} \quad [31a]$$

$$g_y = \frac{d\varphi_y}{d\varphi} \quad [31b]$$

$$g_z = \frac{d\varphi_z}{d\varphi} \quad [31c]$$

From Eq. [29] and Eq. [30] it is seen that

$$g_x + g_y + g_z = 1 \quad [32]$$

The porous electrode material under consideration is isotropic and uniform expansion is assumed in all three directions, i.e. the change in dimensions of the electrode in all three directions is equal and the splitting parameters are constant.

$$g_x = g_y = g_z = {}^1/_3 \quad [33]$$

Also, assuming that the current travels between the separator and the current collector in the x direction, the change in ionic resistance of the porous electrode due to volume change during operation, is given by [32]

$$\frac{R_i}{R_i^0} = \frac{L_x / L_x^0}{(A_x / A_x^0)(\varepsilon / \varepsilon^0)^{1.5}} \quad [34]$$

Here, the subscript $'0'$ indicates initial values, i.e. before the values of the variables before intercalation. The dimensions of the electrode can be derived from Eq. [31] as,

$$\frac{L_x}{L_x^0} = \left(\frac{V}{V^0}\right)^{g_x} \quad [35]$$

$$\frac{A_x}{A_x^0} = \left(\frac{V}{V^0}\right)^{1-g_x} \quad [36]$$

If the porous electrode material considered is anisotropic then g_x needs to be defined accordingly. For the purpose of this work these are considered constant. Also, the cell potential is defined as,

$$E - E^0 = -0.059 \ln\left(\frac{x}{1-x}\right) \quad [37]$$

Chapter 3: RESULTS AND DISCUSSIONS

During intercalation of a porous electrode, it undergoes expansion and the pores are partially filled on account of material being added. If this porous electrode is subjected to de-intercalation, then it undergoes shrinkage and pores are being generated as a result of material being removed. For this study, three cases, similar to the study in Gomadam et al. [40] have been considered. These are, Case – 1: the electrode volume remains constant (swelling coefficient, g = 0) and the porosity changes during intercalation/de-intercalation processes, Case – 2: the porosity remains constant (g = 1) and the volume changes during intercalation/de- intercalation processes and Case – 3: both the porous electrode volume and the porosity change during intercalation/de- intercalation processes. The first two cases are limiting cases as they are not realistic.

Total electrode strain (already dimensionless) examined as a function of volume change and relative compressibility is given by Eq. [13]. Relative compressibility, the ratio of electrode to casing compressibility dictates which of the two, the electrode or the casing is stiffer when compared against each other. When θ is small, it would mean that either the casing is compliant or that the electrode is stiff, whichever the case, the electrode undergoes dimensional change that equals the volume change and when theta is sufficiently large, it would mean that either the casing is stiff or that the electrode is compliant, either way, the electrode does not undergo any dimensional change. Generally since both the electrode and the casing have a finite compressibility, the above mentioned

cases are limiting and fictional. Since theta has a finite value, a fraction of volume expansion goes towards dimensional change and the rest goes towards the change in electrode porosity. It is observed that as theta increases, the electrode undergoes lesser dimensional change for any volume change of the electrode, as expected.

Dimensionless hydrostatic stress is given by the product of hydrostatic stress and the casing compressibility, gives the dimensionless stresses, which is equal to the total electrode strain and hence stresses behave similar to strain. When θ is small, there will be no generation of stresses, because either the casing expands freely i.e. it has infinite compressibility or that the electrode is stiff i.e. it has zero compressibility and when theta is sufficiently large, there will be a large generation of stresses.

Electrode porosity (already dimensionless) is given as a function of volume change and relative compressibility by Eq. [23]. When θ is small, there will be no change in porosity as the electrode will undergoes full expansion without generating any stresses and when theta is sufficiently large, there is a rapid decrease in porosity as dimensional change will be completely restricted and there will only be change in electrode porosity.

The assumption of uniform reaction current, uniform porosity distribution i.e. ε is uniform and no transport limitations inside the solid phase have been made. The volume of the electrode during intercalation can be held constant by encasing it in an infinitely stiff casing. The casing, which does not undergo volume change under the application of stress has zero compressibility ($C_{\mathrm{C}} = 0$) as shown in Figure 3.1a. On the other hand, if the porous material can undergo a full volume expansion when encased in an infinitely compliant casing. This casing which can readily undergo volume change when stress is

applied, has an infinite compressibility ($C_C = \infty$) as shown in Figure 3.1b. Generally, the casing has a finite compressibility ($0 < C_C < \infty$) as shown in Figure 3.1c and due to this, there is a fraction of volume change that goes towards the change in dimensions of the electrode and the remaining fraction of volume change goes towards filling/generation of pores. The results presented herein are for intercalation of a porous electrode which undergoes 100% volume expansion, with constant electrode compressibility (C_E) and varying the casing compressibility (C_C) to match the three cases.

The stress generation inside the porous electrode is calculated by equating Eq. [11] and Eq. [12]. For the first case, the electrode is encased in a stiff casing ($C_C = 0$). This would imply that, the electrode strain is then given by

$$\varphi = 0 \qquad [38]$$

This gives the stress generation inside the porous electrode and these stresses can then be subsequently used for the calculation of porosity through Eq. [24]. For the second case, when the electrode is encased in an infinitely compliant casing ($C_C = \infty$). The casing is offering no resistance to the volume expansion and hence there would be no requirement to fill the pores. There is no stress generation and the porosity as defined by Eq. [24] is then reduce to

$$\varepsilon(\sigma = 0) = \varepsilon^0 \qquad [39]$$

For the third case, since both the electrode and the casing have a finite compressibility, the stress generation, volume change and the change in porosity can be predicted by Eq. [11], Eq. [12] and Eq. [24] respectively. Porous electrode material is enclosed in casing, generally aluminum and steel [45 – 47], but the use of polymers has also been reported, such

as encasing Lithium ion batteries in a polycarbonate tube for underwater usage [48] and using polyurethane and epoxy resin for the protection from vacuum in space [49]. For the present study, both electrode and casing compressibility's are considered constant. Compressibility for porous material is generally between $5 - 80\ \mathrm{GPa}^{-1}$. Compressibility for the casing is calculated by assuming expansion of thin walled spherical vessels and casing material mechanical properties. Aluminum and a Polymer that is five times more compressible than Aluminum are considered as casing material for the study.

The generation of hydrostatic stresses, inside the porous electrode is depicted in Figure 3.2. When the porous electrode is encased in a stiff casing ($C_{\mathrm{C}} = 0$), all of the volume expansion is restricted and all of which is then directed towards the filling of the pores. Since all of the expansion is restricted, stresses of about $1\ \mathrm{GPa}$ are generated. On the other hand, when infinitely compliant casing is used ($C_{\mathrm{C}} = \infty$), there is free expansion of the electrode as the casing does not provide any restriction to volume expansion and thus no stresses are generated. When finitely elastic casings (Aluminum and Polymer) are used, the stress generation is still very large as the electrode undergoes large volume expansion. Since, Aluminum casing ($C_{\mathrm{C}} = 1\ \mathrm{GPa}^{-1}$) is less compressible than the Polymer casing ($C_{\mathrm{C}} = 5\ \mathrm{GPa}^{-1}$), in other words, the former being stiffer than the latter, the stress generation for the former is higher. Aluminum casings generate stresses about $0.175\ \mathrm{GPa}$ weheras Polymer casing generates about $85\ \mathrm{MPa}$ stresses. Stresses generated by the polymer casing are similar to the real time stress measurements in composite silicon electrodes during lithiation measured by Sethuraman et al. [50], where the authors measured compressive stresses of about 70 and $12\ \mathrm{MPa}$, for two different types of binders used in the preparation of the composite silicon electrodes but the stresses

generated when Aluminum casing is used are three times greater in magnitude. Chon et al. [51] observed fracture and fragmentation of the composite amorphous silicon electrode (300% volume expansion) at about 1.5 GPa, which is higher than the stresses predicted here for the electrode that undergoes 100% volume expansion, when Aluminum casing is used and closer to when the casing is infinitely stiff. It is observed that the stresses increase with the increase in change in volume. For an electrode that undergoes 10% volume change like carbon, the stresses produced are about 9.5 and 6.8 MPa respectively for Aluminum ($C_C = 1\ \mathrm{GPa}^{-1}$) and Polymer casing ($C_C = 5\ \mathrm{GPa}^{-1}$), which is of the same order of magnitude as reported by Sethuraman et al [52], of about 10-12 MPa. For an electrode that undergoes 300% volume change like silicon, the stresses produced are about 2 GPa and 0.4 GPa respectively for Aluminum ($C_C = 1\ \mathrm{GPa}^{-1}$) and Polymer casing($C_C = 5\ \mathrm{GPa}^{-1}$). Stresses predicted for this electrode are of the same order of magnitude as reported in Chon et al. [51]. Since Aluminum is stiffer than Polymer, irrespective of the volume change more stresses are generated, as the volume change is being restricted and directed towards the change in porosity. The percentage change in volume for this electrode or the total electrode strain is depicted by Figure 3.3. When the casing on the electrode is stiff ($C_C = 0$), there is no change in strain as the expansion is restricted by the stiff casing and this generates the highest stresses. When the casing is infinitely compliant ($C_C = \infty$), the electrode undergoes a full volume expansion of 100% (twice the original volume at the end of intercalation). When the casing is finitely elastic, in case of Aluminum casing ($C_C = 1\ \mathrm{GPa}^{-1}$) the volume expansion is only about 18% of the actual expansion and in case of Polymer casing ($C_C = 5\ \mathrm{GPa}^{-1}$) the volume expansion is about 43% of the actual expansion. This would imply that about 18% in case

of Aluminum casing and 43% in case of Polymer casing, of the total volume expansion went into the change in dimensions of the electrode and the rest of the fraction was consumed for filling the pores in the porous electrode material. As mentioned earlier, since Aluminum casing $(C_C = 1\ \text{GPa}^{-1})$ is comparatively stiffer than the Polymer casing$(C_C = 5\ \text{GPa}^{-1})$, it is able to restrict more of the volume change and direct it towards the change in porosity. It is observed that, if the casing used is comparatively stiffer, the fraction of volume change that goes into changing the dimensions of the electrode decreases. As the casing used gets comparatively stiffer, it restricts the volume expansion of the electrode and hence more stresses are generated, irrespective of the total volume expansion. The change in porosity of the electrode during intercalation is depicted in Figure 3.4. Most of the pores in the electrode are filled during intercalation, when the casing is stiff $(C_C = 0)$. This is because all of the volume expansion is restricted by the stiff casing and is directed towards filling of the pores, which in turn generates large stresses. Comparatively, when the casing is finitely elastic, the pores are not filled as rapidly as the casing does not provide enough resistance to the volume change of the electrode and hence not all of the intercalate coming into the volume acts to fill the pores. Since Aluminum casing $(C_C = 1\ \text{GPa}^{-1})$ is stiffer than the Polymer casing$(C_C = 5\ \text{GPa}^{-1})$, comparatively the electrode undergoes larger change in porosity with the former, similar to the indication given by Figure 3.3. On the other hand, when the casing is infinitely compliant ($C_C = \infty$), there is no resistance to the volume change of the electrode and free expansion occurs due to which there is no generation of stresses and hence no change in the porosity of the electrode. It is observed that, if the casing used is comparatively stiffer, the fraction of volume change that goes into changing of porosity

increases and more of volume of the intercalate coming into the electrode goes into filling the pores, irrespective of the total volume expansion. As the casing used gets comparatively stiffer, more stresses are generated, which directs most of the volume change into porosity change. The swelling coefficient 'g' is calculated using Eq. [26], and it is depends on the volume change of the electrode, the compressibility of the casing and the compressibility of the electrode. Figure 3.5 shows the swelling coefficient for both Aluminum casing ($C_C = 1\ \mathrm{GPa}^{-1}$) and Polymer casing ($C_C = 5\ \mathrm{GPa}^{-1}$). It should be noted that when volume change of the electrode is not large enough for electrode material like carbon, the swelling coefficient is sufficiently constant, which would indicate that a constant fraction of volume expansion would go into dimensional change and the rest would go into porosity change, but when the volume change is sufficiently large (as shown) it is seen that the swelling coefficient is no longer a constant value but changes during intercalation and this in turn would affect the cell potential. In this case the curves suggest that during initial intercalation there is change in porosity and as intercalation continues, the material undergoes dimensional changes. Both, Aluminum and Polymer show similar behavior, this is because the casing is comparatively less compressible than the porous electrode i.e. they are comparatively stiffer than the porous electrode and offers more resistance to the volume change, hence initially directing the volume change towards the change in porosity. It is also seen that during de-intercalation, after the electrode is fully intercalated, the material follows the same pattern and there is no change in the swelling coefficient. The electrode under consideration is assumed to only have Ionic resistance and the effect of volume expansion (100%) is high on the ionic resistance. This is reflected in the Figure 3.6, a plot of the dimensionless ionic resistance.

It is seen that, when the casing is stiff ($C_C = 0$), all the pores are filled faster, i.e. the electrolyte is pushed out of the electrode, hence there is a rapid rise in ionic resistance as compared to when the casing is elastic, but when the casing is infinitely compliant ($C_C = \infty$) the porosity remains constant during volume expansion, this allows the amount of electrolyte to remain the same but as the volume increases, the dimensions and hence the area of the electrode increases which decreases the ionic resistance during expansion. Aluminum casing ($C_C = 1\ \mathrm{GPa}^{-1}$) offers more resistance than the Polymer casing($C_C = 5\ \mathrm{GPa}^{-1}$) as the former is stiffer than the latter and undergoes larger change in porosity and subsequently lesser change in dimensions. The Figure 3.7 shows the cell voltage for this electrode. Since the volume change of the electrode is significant, there is rapid increase in resistance of the electrode and hence there is appreciable difference in the potentials between all three cases. For comparison Nernst potential with a constant ohmic drop is also shown. It is seen that when a stiff casing is used the cell voltage deviates the most as compared to when compliant casing is used. This implies that if volume change is not accurately accounted for, then accurate prediction of electrochemical performance of the porous electrode cannot be made. Since Aluminum casing ($C_C = 1\ \mathrm{GPa}^{-1}$) is stiffer than the Polymer casing ($C_C = 5\ \mathrm{GPa}^{-1}$), the deviation of cell potential is greater. The initial value of swelling coefficient with respect to relative compressibility (θ) is shown in Figure 3.8. The diamond indicates the initial value of the swelling coefficient for the results with the Polymer casing and the square indicates the initial value of the swelling coefficient for the results with Aluminum casing shown herein. This figure indicates that if relative compressibility (θ), is small the electrode material will tend to direct the volume change to dimensional change and if it is large the electrode material

will tend to direct the volume change into change in porosity. For cases discussed earlier, the relative compressibility is greater than 1 ($\theta > 1$), which means that the casing is comparatively stiffer than the electrode. Due to this the casing provides enough resistance to the volume change of the electrode and the intercalate volume is initially put towards filling the pores. It is also seen that if the casing is sufficiently stiff there will be no dimensional change initially and all the intercalate volume will be put towards the change in porosity and vice versa if the casing is sufficiently compliant there will be no change in porosity initially and all the intercalate volume will go towards the change in dimensions of the porous electrode.

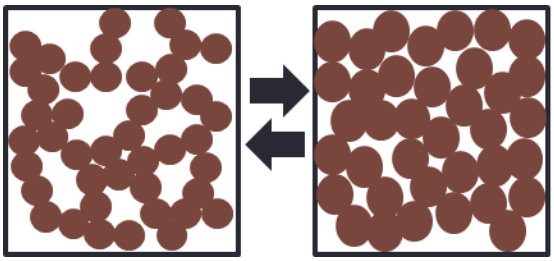

$$C_C = 0$$

Figure 3.1a: Depicts Case #1 when the porous electrode is enclosed within an infinitely stiff casing, during intercalation there is no change in the volume of the electrode (g = 0)

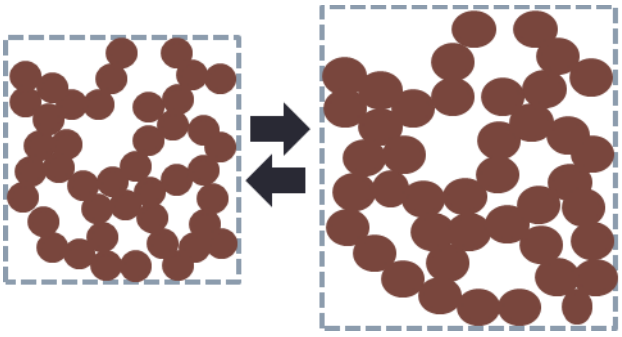

$$C_C = \infty$$

Figure 3.1b: Depicts Case # 2 when the porous electrode is enclosed in a complaint casing, during intercalation there is only change in dimension of the electrode and the porosity of the electrode does not change (g = 1)

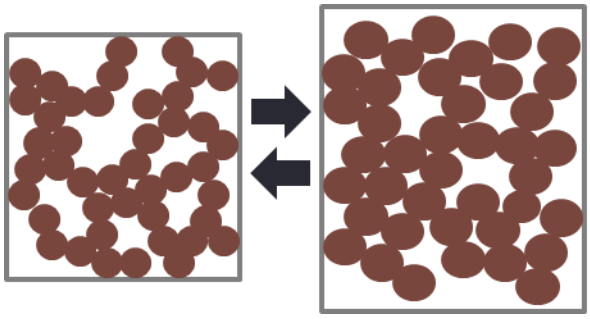

$$0 < C_C < \infty$$

Figure 3.1c: Depicts Case # 3 when the porous electrode is enclosed in a finitely elastic casing, during intercalation both the dimensions and the porosity of the electrode change (0 < g < 1)

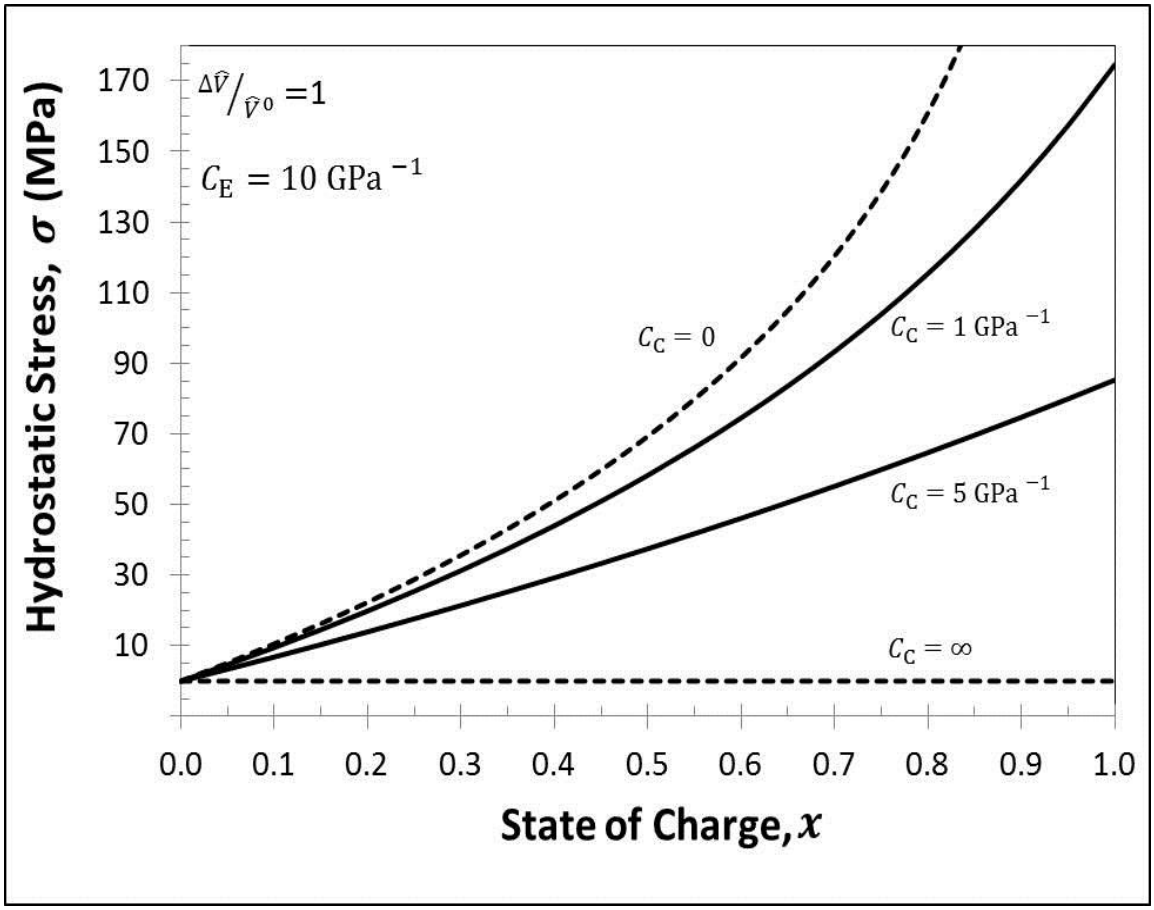

Figure 3.2: Generation of Hydrostatic Stresses during intercalation for $\Delta\hat{V}/\hat{V}^0 = 1$ with $C_E = 10\ \text{GPa}^{-1}$. For four cases, Case #1when stiff casing is used i.e. $C_C = 0$ (▬▬), Case # 2 when infinitely elastic casing is used i.e.$C_C = \infty$ (▬▬), Case # 3 when finitely elastic, Aluminum casing is used i.e. $C_C = 1\ \text{GPa}^{-1}$ (▬) and Case # 4 when finitely elastic, Polymer casing is used i.e. $C_C = 5\ \text{GPa}^{-1}$ (▬)

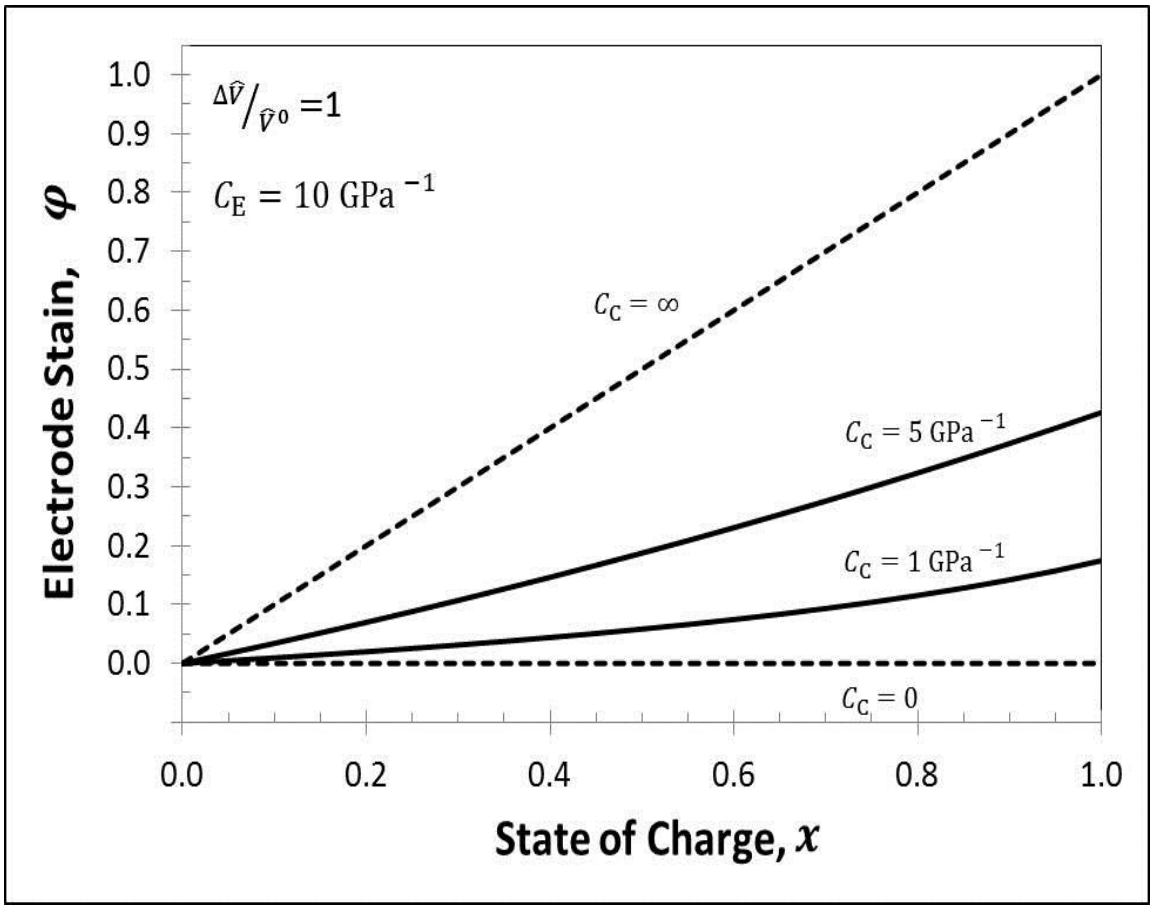

Figure 3.3: Change in Total Electrode Strain during intercalation for $\Delta\hat{V}/\hat{V}^0 = 1$ with $C_E = 10\ \text{GPa}^{-1}$. For four cases, Case #1when stiff casing is used i.e. $C_C = 0$ (- -), Case # 2 when infinitely elastic casing is used i.e.$C_C = \infty$ (- -), Case # 3 when finitely elastic, Aluminum casing is used i.e. $C_C = 1\ \text{GPa}^{-1}$ (—) and Case # 4 when finitely elastic, Polymer casing is used i.e. $C_C = 5\ \text{GPa}^{-1}$ (—)

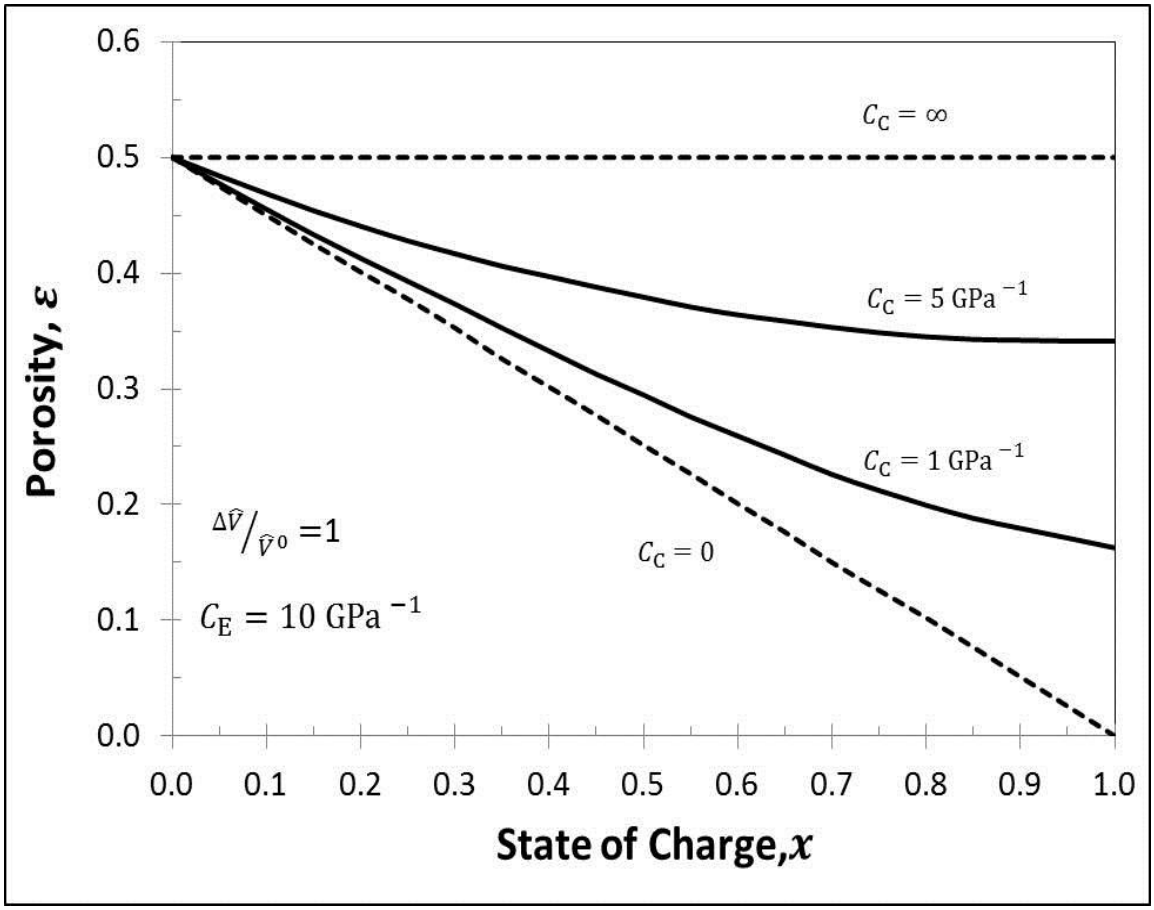

Figure 3.4: Change in Porosity during intercalation for $\Delta\hat{V}/\hat{V}^0 = 1$ with $C_E = 10\text{GPa}^{-1}$. For four cases, Case #1when stiff casing is used i.e. $C_C = 0$ (- - -), Case # 2 when infinitely elastic casing is used i.e.$C_C = \infty$ (- - -), Case # 3 when finitely elastic, Aluminum casing is used i.e. $C_C = 1\ \text{GPa}^{-1}$ (—) and Case # 4 when finitely elastic, Polymer casing is used i.e. $C_C = 5\ \text{GPa}^{-1}$ (—)

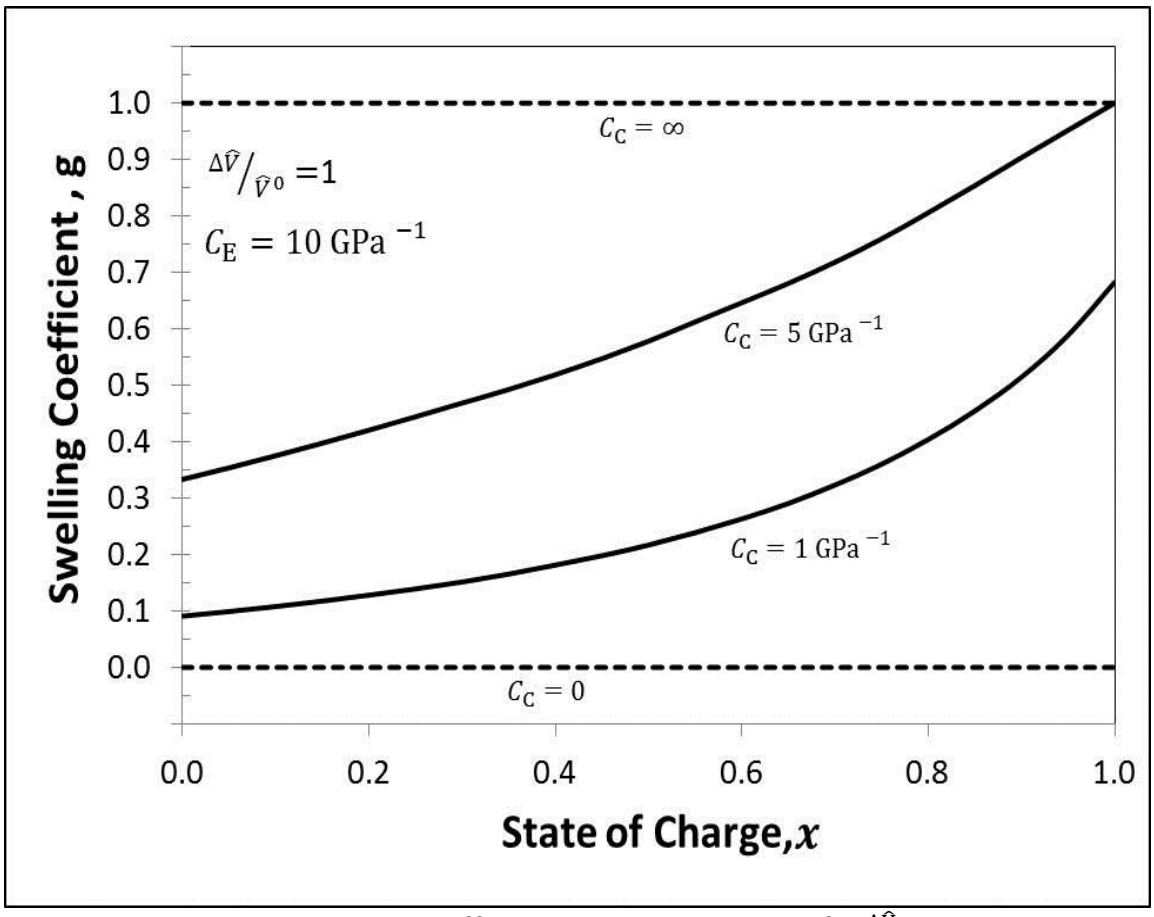

Figure 3.5: Change in swelling coefficient during intercalation for $^{\Delta\hat{V}}/_{\hat{V}^0} = 1$ with $C_E = 10\text{GPa}^{-1}$. For four cases, Case #1when stiff casing is used i.e. $C_C = 0$ (--), Case # 2 when infinitely elastic casing is used i.e.$C_C = \infty$ (--), Case # 3 when finitely elastic, Aluminum casing is used i.e. $C_C = 1\ \text{GPa}^{-1}$ (—) and Case # 4 when finitely elastic, Polymer casing is used i.e. $C_C = 5\ \text{GPa}^{-1}$(—)

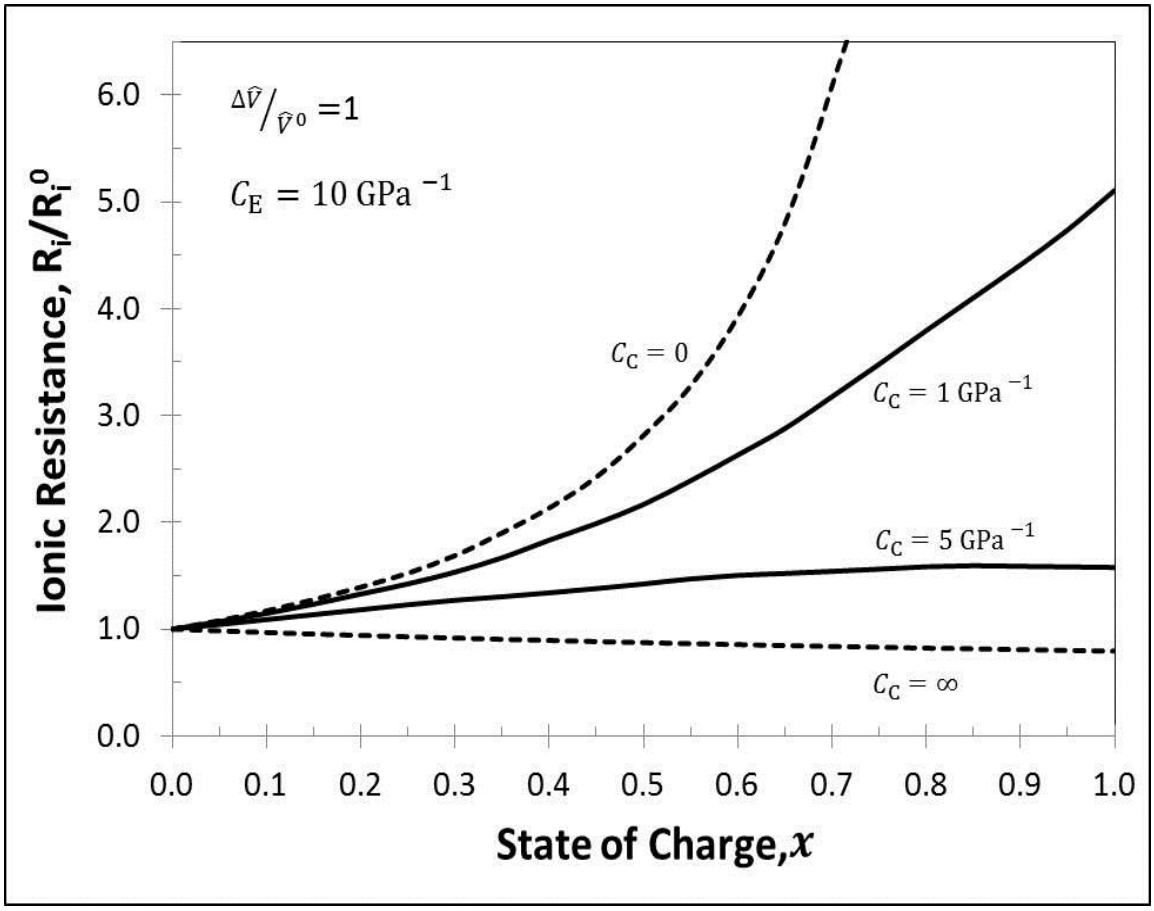

Figure 3.6: Ionic Resistances during intercalation for $\Delta\hat{V}/\hat{V}^0 = 1$ with $C_E = 10\text{GPa}^{-1}$. For four cases, Case #1when stiff casing is used i.e. $C_C = 0$ (**- -**), Case # 2 when infinitely elastic casing is used i.e.$C_C = \infty$ (**- -**), Case # 3 when finitely elastic, Aluminum casing is used i.e. $C_C = 1\ \text{GPa}^{-1}$ (**—**) and Case # 4 when finitely elastic, Polymer casing is used i.e. $C_C = 5\ \text{GPa}^{-1}$ (**—**)

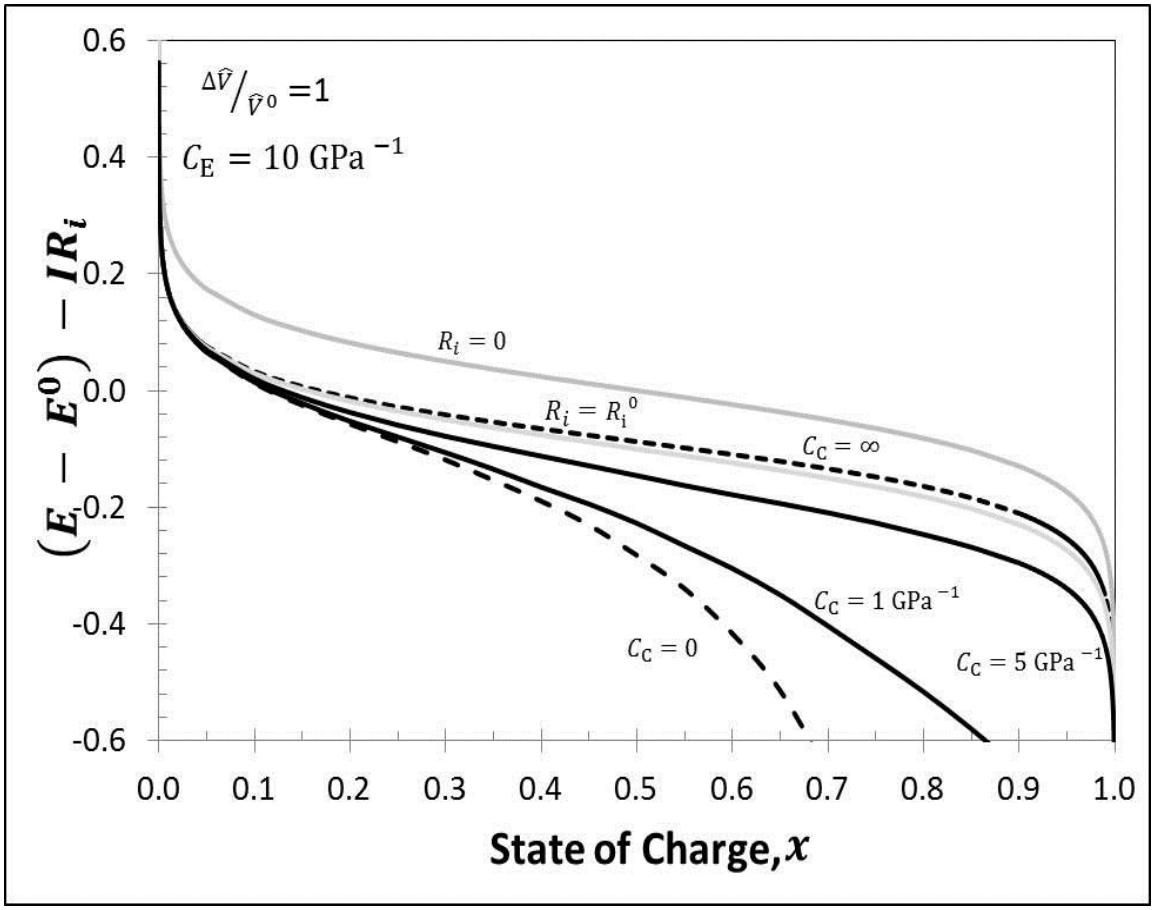

Figure 3.7: Cell Voltage during intercalation for $\Delta\hat{V}/\hat{V}^0 = 1$ with $C_E = 10\text{GPa}^{-1}$. For four cases, Case #1when stiff casing is used i.e. $C_C = 0$ (**- -**), Case # 2 when infinitely elastic casing is used i.e.$C_C = \infty$ (**- -**), Case # 3 when finitely elastic, Aluminum casing is used i.e. $C_C = 1\ \text{GPa}^{-1}$ (**—**) and Case # 4 when finitely elastic, Polymer casing is used i.e. $C_C = 5\ \text{GPa}^{-1}$ (**—**). For comparison Nernst potential with constant ohmic drop is shown (—)

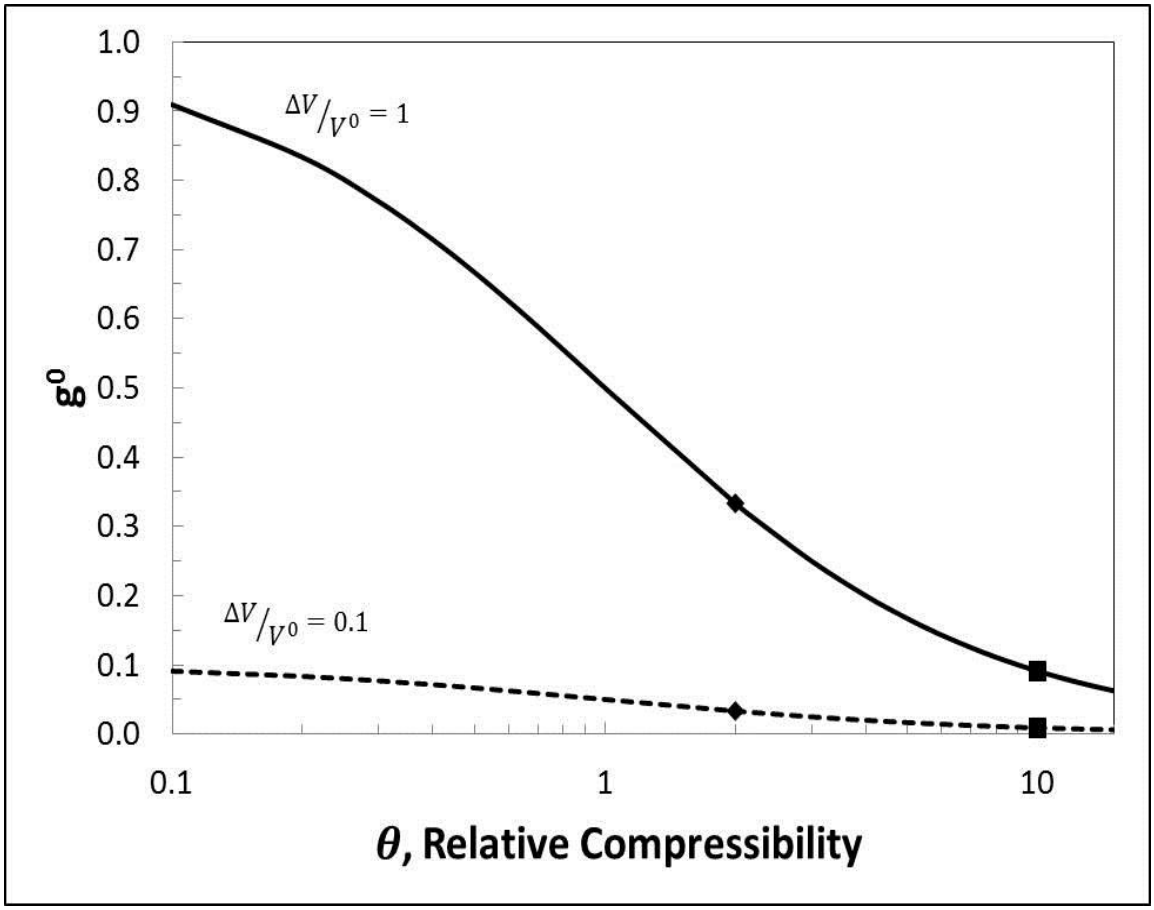

Figure 3.8: Initial value of swelling coefficient versus relative compressibility. (■) is when finitely elastic, Aluminum casing $C_C = 1$ GPa $^{-1}$ is used and (◆) is when finitely elastic, Polymer casing is $C_C = 5$ GPa $^{-1}$ is used

Table 3.1: Material attributes assigned to the electrode volume under consideration

Assigned properties	Values
Compressibility of the Electrode $(\boldsymbol{C_E})$	10 GPa^{-1}
Compressibility of Aluminum Casing	1 GPa^{-1}
Compressibility of Polymer Casing	5 GPa^{-1}
Compressibility of Stiff Casing	1.25 EPa^{-1}
Fraction of Volume, comprising the x direction (g_x)	0.334
Initial Porosity $(\boldsymbol{\varepsilon^0})$	0.5
Initial Resistance $(\boldsymbol{R_i^0})$	0.1 Ω
Initial Volume $(\boldsymbol{V^0})$	10 cm^3
Initial Molar Volume $(\boldsymbol{\widehat{V}^0})$	12.059 cm^3/mol
Poisson's Ratio for Aluminum [53]	70 GPa
Young's Modulus for Aluminum [53]	0.35

Chapter 4: CONCLUSIONS

A modeling approach has been established to predict the extent to which volume change of the solid phase translates into the porosity and volume change of the porous electrode and predict stress generation within the electrode due to this change. Consecutively a mathematical model has been developed to describe volume changes of the porous electrode when it undergoes 100% volume change. The design dependent parameter g is tracked throughout the electrode process, in order to track the individual magnitudes of changes in dimensions and porosity. The compressibility of the electrode material and the casing, which have to be obtained experimentally are approximated.

Using material balance over the electrode solid phase and constitutive law from rock mechanics, stress-strain relationships needed to predict porosity and volume changes have been established. This approach can also be integrated into a complete battery models based on porous electrode theory, to extend the existing porous electrode models to accurately include volume change effects.

Chapter 5: FUTURE WORK

A 0-D model has been developed to describe the volume changes in a porous electrode and predict the stresses generated therein. The next step would be to extent our analysis to a complete battery model, in which the two porous electrodes (positive and negative) sandwich the electrolyte membrane/separator which allows for ion transport when electro-chemical reactions occur in the electrodes. The electrodes are connected externally to complete the circuit. The model development for such a battery model in shown in APPENDIX E. A representative diagram of such a model is shown in Figure 5.1.

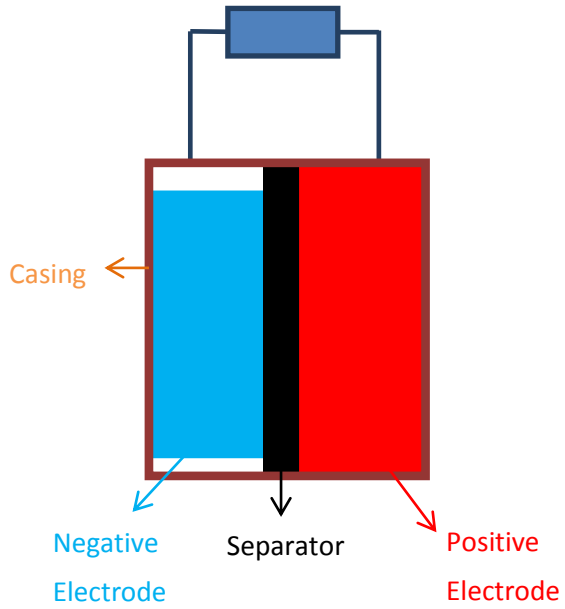

Figure 5.1: A representative diagram of the battery

During volume expansion in the electrode, the electrode material interacts with itself. The understanding of these interactions between the micro/nano structures is important. The

present model is simplified due to the assumptions of uniform reaction distribution, isotropic material and uniform reaction rates. The next step would be to relax these assumptions.

The understanding of interactions between the micro/nano structures is important as they lead to higher stress generation. For the purpose of modeling simple geometric shapes have been often been rendered to porous material, which in reality is not the case. Guan et al. [54] used X-ray Computed nano-Tomography to visualize the 3-D microstructure of a SOFC by characterizing key parameters like, volume ratio of the active/inactive species, porosity, three-phase boundary length, specific interfacial area and conductivity of the electrode meanwhile Garzon et al. [55] used X-ray Computed micro and nano-Tomography to study the internal morphological changes in the PEM fuel cell membranes. Hence using XCT a detail micro/nanostructure of the porous electrode can be generated and used as a template for realistic geometries, instead of generating suitable electrode geometries that mimic realistic electrode geometries. These templates can then be assigned to the porous microstructure to help develop better Pseudo 2-D models which would carry out the aforementioned analysis. It is also possible to carry out fracture analysis using XCT similar to Feser et al [56] and Pendleton et al [57].

During model development the compressibility data for both the electrode and casing were estimated. The compressibility of both the electrode material and the casing, varies with stress generated within the electrode volume, to get an accurate prediction of stress generation it is then essential that these parameters be experimentally measured and used for simulation purposes. The compressibility of both the electrodes and the casing

can be measured experimentally [58, 59], by coupling a mechanical testing device to a high resolution X-ray microscope and subsequently using Digital Volume Correlation (DVC) or Digital Image Correlation (DIC) to identify the displacements. Wherein the mechanical testing device will apply finite loads on the composite porous material and the XCT will generate 3-D images of the porous material. Using DVC or DIC on these 3-D images, the change in volume can then be calculated, thus establishing the dependence of compressibility on stress for the porous material.

Figure 5.2: Xardia's VersaXRM-520 used for X-ray Computed Tomography [61]

Figure 5.2 shows the Xardia's VersaXRM-520, one of the most versatile XCT available from Xardia, commonly used in laboratories. After compressibility data for various electrode materials and casings are identified, reevaluation of the battery model is required. This would enable realistic prediction of stresses, inside the battery, during electrode processes.

REFERNECES

1. . J.M. Tarascon and M. Armand, “Issues and challenges facing rechargeable lithium batteries”, Nature 414 (2001)
2. R. E. Garcıa, Y. M. Chiang, W. C. Carter, P. Limthongkul and C. M. Bishop,” Microstructural Modeling and Design of Rechargeable Lithium-Ion Batteries”, J. Electrochemical Society 152 (1), pp. A255-A263 (2005)
3. J. Newman and K. E. Thomas-Alyea, Electrochemical systems, 3rd ed, John Wiley & Sons, New York (2004)
4. C. K. Chan, H. Peng, G. Liu, K. McIlwrath, X. F. Zhang, R. A. Huggins and Y. Cui, “High-performance lithium battery anodes using silicon nanowires”. Nature Nanotechnology 3 (2008)
5. T. Song, J. Xia, J. H. Lee, D. H. Lee, M. S. Kwon, J. M Choi, J. Wu, S. K. Doo, H. Chang, W. I. Park, D. S. Zang, H. Kim, Y. Huang, K. C. Hwang, J. A. Rogers and U. Paik, “Arrays of sealed Silicon Nanotubes as anodes for Lithium Ion Batteries”. Nano Letters 10: pp 1710-1716 (2010)
6. C. M. DeLuca, K. Maute and M. L. Dunn, “Effects of electrode particle morphology on stress generation in silicon during lithium insertion”. J. Power Sources 196: pp 9672– 9681 (2011)
7. F. Yang, “Insertion-Induced breakage of material” J. Applied Physics 108: pp. 073536-073541(2010)
8. J. Le, Z. Bazant and M. Bazant, “Subcritical crack growth law a nd its consequences for lifetime statistics of quasibrittle structures” J. Physics D: Applied Physics 42: pp. 214008-214016 (2009)
9. S. Kalnaus, K. Rhodes and C. Daniel, “A study of Lithium ion intercalation induced fracture of silicon particles used as anode material in Li-ion battery” J. Power Sources 196: pp. 8116-8124 (2011)
10. K. Zhao, M. Pharr, J. J. Vlassak and Z. Suo,”Fracture of electrodes in lithium-ion batteries caused by fast charging” J. Applied Physics 108: pp. 073517-073523 (2010)
11. K. Zhao, M. Pharr, J. J. Vlassak and Z. Suo,”Inelastic hosts as electrodes for high-capacity lithium-ion batteries” J. Applied Physics 109: pp. 016110-016113 (2011)
12. G.A. Nazri and G. Pistoia, Springer Science and Buisness media, New York (2009). pp. 117
13. M. N. Obrovac, L. Christensen, D. B. Le and J. R. Dahn, “Alloy Design for Lithium-Ion Battery Anodes” J. Electrochemical Society 154(9): pp. A849-A855 (2007)
14. J. Christensen and J. Newman, “Stress generation and fracture in lithium insertion materials” J. of Solid State Electrochemistry 10 (5), pp 293-319 (2006)
15. M. Doyle and J. Newman, “The use of mathematical modeling in the design of lithium/polymer battery systems” Electrochemica Acta 40(13): pp. 2191-2196 (1995)

16. M. Doyle and J. Newman, ”Modeling the performance of rechargeable lithium-based cells: design correlations for limiting cases” J. Power Sources 54: pp. 46-51 (1995)
17. J. Newman, K. E. Thomas, H. Hafezi and D.R. Wheeler, “Modeling of lithium-ion batteries” J. Power Sources 191-121: pp. 838-843 (2006)
18. J. Christensen and J. Newman, “A mathematical model of stress generation and fracture in Lithium Manganese Oxide” J. Electrochemical Society 153(6):pp. A1019-A1030 (2006)
19. X. Zhang, W. Shyy and A. M. Sastry, ” Numerical Simulation of Intercalation-Induced Stress in Li-Ion Battery Electrode Particles” J. Electrochemical Society 154(10): pp. A910-A916 (2007)
20. J. Park, W. Lu and A. M. Sastry, "Numerical simulation of stress evolution in lithium manganese dioxide particles due to coupled phase transition and intercalation” J. Electrochemical Society 158(2): pp. A201-A206 (2011)
21. R. Deshpande, Y. Cheng and M. Verbrugge, “Modeling diffusion-induced stress in nanowire electrode structures” J. Power Sources 195: pp. 5081-5088 (2010)
22. Y. Cheng and M. Verbrugge, “The influence of surface mechanics on diffusion induced stresses within spherical nanoparticles” J. Applied Physics 104: pp. 083521-083526 (2008)
23. Y. Cheng and M. Verbrugge, “Diffusion-induced stress, interfacial charge transfer, and criteria for avoiding crack initiation of electrode particles” J. Electrochemical Society 157(4): pp. A508-A516 (2010)
24. J. S. Newman and C. W. Tobias, “Theoretical analysis of current distribution in porous electrodes” J. Electrochemical Society 109(12): pp. 1183-1191 (1962)
25. R. C. Alkire, E. A. Grens II and C. W. Tobias, “A Theory for porous electrodes undergoing structural change by anodic dissolution” J> Electrochemical Society: Electrochemical Science 116(10): pp.1328-1333 (1969)
26. J. S. Dunning, D. N. Bennion and J. Newman, “Analysis of porous electrodes with sparingly soluble reactants II. Variable solution properties, convection and complexing” J. Electrochemical Society: Electrochemical Science and Technology 120(7):pp.90-913 (1973)
27. T. Fuller, M. Doyle and J. Newman, “Simulation and optimization of the dual lithium ion insertion cell” J. Electrochemical Society 141(1):pp. 1-10 (1994)
28. M. Doyle, J. Newman, A. S. Gozdz, C. N. Schmutz and J-M Tarascon, “Comparison of modeling predictions with experimental data from plastic lithium ion cells” J. Electrochemical Society 143(6) : pp. 1890-1903 (1996)
29. M. Jain, and J. W. Weidner,” Material Balance Modification in One-Dimensional Modeling of Porous Electrodes” J. Electrochemical Society 146 (4):pp. 1370-1374 (1999)
30. M. Jain, N. Ganesan, G. J. Rudolph and J. W. Weidner,” Analysis of a Lithium/Thionyl Chloride Battery under Moderate-Rate Discharge” J. Electrochemical Society 146 (11):pp. 4023-4030 (1999)
31. L. Cai, Y. Dai, m. Nicholson, R. E. White, K. Jagannathan and G. Bhatia, “Life modelinf of lithium ion cell with a spinel-based cathode” J. Power Sources 221: pp. 191-200 (2013)
32. P.M. Gomadam and J.W. Weidner, “Modeling Volume Change in Porous Electrodes” J. Electrochem. Soc, 153 (1), A175-A186 (2006)

33. Zhang, X.C., Sastry, A.M., and W. Shyy, "Intercalation-induced stress and heat generation within single lithium-ion battery cathode," J. Electrochemical Society v.155 (7): pp.A542-A552 (2008)
34. R. Deshpande, Y. T. Cheng, M. W. Verbrugge and A. Timmons,"Diffusion induced stresses and strain energy in a phase transforming spherical electrode particle" J. Electrochemical Society v. 158 (6): pp. A718-A724 (2011)
35. Y. F. Gao, and M. Zhou., "Strong stress enhanced diffusion in amorphous lithium alloy nanowire electrode" J. Applied Physics 109: pp. 014310-014316 (2011)
36. I. Ryu, J. W. Choi, Y. Cui and W. D. Nix," Size dependent fracture of Silicon nanowire battery anodes" Journal of the Mechanics and Physics of Solids 59: pp. 1717-1730 (2011)
37. Y. Yao, M. T. McDowell, I. Ryu, H. Wu, N. Liu, L. Hu, W. D. Nix and Y. Cui," Interconnected silicon hollow nanospheres for lithium ion battery anodes with long cycle life" Nano Letters 11: pp. 2949-2954 (2011)
38. W. L. Wang, S. Lee, and J. R. Chen," Effect of chemical stress on diffusion in a hollow cylinder" J. Applied Physics 91 (12) :pp. 9584-9590 (2002)
39. R. Krishnan, T. M. Lu and N. Koratkar,"Functionally strain graded nanoscoops for high powered Li-ion battery anodes". American Chemical Society: Nano Letters 11: pp. 377-384 (2011)
40. S. Renganathan, G. Sikha, S. Santhanagopalan and R. E. White,"Theoretical analysis of stress in a lithium ion cell" J. Electrochemical Society 157(2): pp. A155-A163 (2010)
41. H. H. Liu, J. Rutqvist and J. G. Berryman," On the relationship between stress and elastic strain for porous and fractured rock" International Journal of Rock Mechanics & Mining Sciences, 46: pp.289-296 (2009)
42. R. Ciz, S. A. Shapiro, "Stress-dependent anisotropy in transversely isotropic rocks: Comparison between theory and laboratory experiment on shale", Geophysics 74: pp. D7-D12 (2009)
43. Y. Zhao, H. H. Liu, "An Elastic Stress–Strain Relationship for Porous Rock under Anisotropic Stress Conditions", Rock Mech Rock Eng. 45: pp. 389-399 (2012)
44. M. Abramowitz and I. A. Stegun. Handbook of Mathematical Functions. Chapter 5, New York: Dover Publications, 1965
45. Application of Life-Cycle Assessment to Nanoscale Technology: Lithium Ion Batteries for electric Vehicles. United States Environment Protection Agency, 2013
46. T. O'Hara and M. Wesselmark,"Battery technologies, A general overview and focus of lithium ion".
47. K. Kohno, Y. Koishikawa, Y. Yagi and T. Horiba, "Development of and Aluminum-laminated lithium ion battery for hybrid electric vehicle application" Journal of Power Sources 185:pp.554-558 (2008)
48. D. R. Pendergast, E. P. DeMauro, M. Fletcher, E. Stimson and J. C. Mollendrof, " A rechargeable lithium-ion battery module for underwater use" Journal of Power Sources 196: pp.793-800 (2011)
49. M. Uno, K. Ogawa, Y. Takeda, Y. Sone, K. Tanka, M. Mita and H. Saito, " Development and on-orbit operation of lithium-ion pouch battery for small scientific satellite REIMEI" Journal of Power Sources 196:pp 8755-9763 (2011)
50. V. A. Sethuraman, A. Nguyen, M. J. Chon, S. P. V. Nadimpalli, H. Wang, D. P.

Abraham, A. F. Bower, V. B. Shenoy and P. R. Guduru, “Stress Evolution in Composite Silicon Electrodes during Lithiation/Delithiation”, Journal of Electrochemical Society 160 (4): pp A739-A746 (2013)
51. M. J. Chon, V. A. Sethuraman, A. McCormick, V. Srinivasan and P. R. Guduru, “Real-Time Measurement of Stress and Damage Evolution during Initial Lithiation of Crystalline Silicon” Physical Review Letters, 107: pp.045503 (2011)
52. V. A. Sethuraman, N. Van Winkle, D. P. Abraham, A. F. Bower and P.R. Guduru, “Real-time stress measurements in lithium-ion battery negative-electrodes” Journal of Power Sources 206:pp.334-342 (2012)
53. M. F. Ashby, Materials selection in mechanical design, 4th ed., Elsevier, Maryland (2011)
54. Y. Guan, W. Li, Y. Gong, G. Liu, X. Zhang, J. Chen, J. Gelb, W. Yun, Y. Xiong, Y. Tian and H. Wang, “Analysis of the three-dimensional microstructure of a solid-oxide fuel cell anode using nano X-ray tomography” Journal of Power Sources 196: pp. 1915–1919 (2011)
55. F. H. Garzon, S.H. Lau, J. R. Davey, and R. L. Borup,” Micro And Nano X-Ray Tomography Of PEM Fuel Cell Membranes After Transient operation”. ECS Trans. **11(1)**: pp. 1139-1149 (2007)
56. M Feser, J Gelb, H Chang, H Cui, F Duewer, S H Lau, A Tkachuk And W Yun,” Sub-micron resolution CT for failure analysis and process development” Meas. Sci. Technol. **19:** pp.094001-094009 (2008)
57. Tyler Pendleton, Luke Hunter and S H Lau,” Noninvasive Failure Analysis of Passive Electronic Devices in Wireless Modules using X-ray Micro tomography (MicroCT)” ISTFA 2008: Proceedings from the 34th International Symposium for Testing and Failure Analysis November 2-6, 2008, Portland, Oregon USA
58. J. D. Lin, H. Ozcoban, J. P. Greene, A. T. Jang, S. I. Djomehri, K. P. Fahey, L. L. Hunter, G. A. Schneider and S. P. Ho, “Biomechanics of a bone-periodontal ligament-tooth fibrous joint”, Journal of Biomechanics, 46: pp. 443-449 (2013)
59. A. Germaneau, P. Doumalin and J. C. Dupre,”Comparison between X-ray micro-computed tomography and optical scanning tomography for full 3D strain measurement by digital volume correlation”, NDT&E International, 41: pp. 407-415 (2008)
60. R. R. Craig Jr. Mechanics of Materials. Chapter 9-Thin walled pressure vessels pp. 608. Third edition. New Jersey: John Wiley & sons, 2011
61. http://www.xradia.com/products/versaxrm-520.php

APPENDIX A: Derivation of Porosity

Substituting Eq. [20] and Eq. [21] in Eq. [19] gives:

$$\frac{d}{d\sigma}(1-\varepsilon)+(1-\varepsilon)C_c=\left[\frac{Q^{max}}{Q^{max}}\right]\frac{C_c}{[1+\sigma C_c]}\left[1+\frac{C_E}{C_c}exp(-C_E\sigma)\right] \quad [A1]$$

Rewriting Eq. [A1] as,

$$\frac{d}{d\sigma}(1-\varepsilon)+(1-\varepsilon)C_c=\frac{C_c(1-\varepsilon^0)}{[1+\sigma C_c]}\left[1+\frac{C_E}{C_c}exp(-C_E\sigma)\right] \quad [A2]$$

Substituting Eq. [14] in [A2],

$$\frac{d\varepsilon}{d\sigma}-(1-\varepsilon)C_c=-C_c(1-\varepsilon^0)\frac{[1+\theta\ exp(-C_E\sigma)]}{[1+\sigma C_c]} \quad [A3]$$

The general solution for

$$y'+P(x)y=Q(x) \quad [A4]$$

Is given as,

$$y(x)=\ e^{-\int P(x)dx}\left\{\int Q(x)e^{\int P(x)dx}\,dx+c\right\} \quad [A5]$$

Comparison of Eq. [A3] with Eq. [A4], results in the definition of the variables as

$$P(x)=\ C_c \quad [A6]$$

$$Q(x)=C_c-C_c(1-\varepsilon^0)\frac{[1+\theta\ exp(-C_E\sigma)]}{[1+\sigma C_c]} \quad [A7]$$

Using Eq. [A7], [A8] in [A6], the porosity can be given as

$$\varepsilon(\sigma) = e^{-\int C_c d\sigma} \left\{ \int \left(C_c - C_c(1-\varepsilon^0) \frac{[1+\theta\ exp(-C_E\sigma)\ ]}{[1+\sigma C_c]} \right) e^{\int C_c d\sigma}\ d\sigma + c \right\} \qquad [A8]$$

Eq. [A8] then results into,

$$\varepsilon(\sigma) = 1 - (1-\varepsilon^0) e^{(-1-\sigma C_c)} Ei(1, -1-\sigma C_c) - \theta(1-\varepsilon^0)\ e^{(-1+\theta\ -\sigma C_c)} Ei(1, -1+\theta + (-1+\theta\ )\sigma C_c)\ + c e^{(-\sigma C_c)} \qquad [A9]$$

APPENDIX B: Derivation of Swelling Coefficient

Substituting Eq. [12] in Eq. [21] and differentiating the resulting equation gives,

$$\frac{dV}{d\sigma} = V^0 C_c \qquad \text{[B1]}$$

The porosity-stress relationship is given by Eq. [A2] as,

$$\frac{d}{d\sigma}(1-\varepsilon) + (1-\varepsilon)C_c = \frac{C_c(1-\varepsilon^0)}{[1+\sigma C_c]}[1 + \theta exp(-C_E\sigma)\,] \qquad \text{[B2]}$$

Using Eq. [B1] and Eq. [B2],

$$\frac{dV}{d(1-\varepsilon)} = \frac{V^0(1+\sigma C_c)}{(1-\varepsilon^0)[1+\theta exp(-C_E\sigma)\,]-(1-\varepsilon)(1+\sigma C_c)} \qquad \text{[B3]}$$

Eq. [B3] can be re-written as,

$$\frac{(1-\varepsilon)}{d(1-\varepsilon)}\frac{dV}{V} = \frac{(1-\varepsilon)}{(1-\varepsilon^0)[1+\theta exp(-C_E\sigma)\,]-(1-\varepsilon)(1+\sigma C_c)} \qquad \text{[B4]}$$

Using Eq. [B4],

$$1 + \frac{(1-\varepsilon)}{d(1-\varepsilon)}\frac{dV}{V} = \frac{(1-\varepsilon^0)[1+\theta exp(-C_E\sigma)\,] -(1-\varepsilon)\sigma C_c}{(1-\varepsilon^0)[1+\theta exp(-C_E\sigma)\,]-(1-\varepsilon)(1+\sigma C_c)} \qquad \text{[B4]}$$

Now, the Swelling coefficient defined by Eq. [26], gives

$$g = \frac{(1-\varepsilon)}{(1-\varepsilon^0)[1+\theta exp(-C_E\sigma)\,] -(1-\varepsilon)\sigma C_c} \qquad \text{[B5]}$$

APPENDIX C: Calculation of constant Compressibility of the casing

Stresses generated in a thin spherical pressure vessel is given as [60],

$$\sigma = \frac{P}{2}\frac{r}{t} \quad \text{[C1]}$$

Here, P, r and t are respectively the ambient pressure, radius and thickness of sphere under consideration. The strain due to volume expansion is then given as,

$$\varphi = \frac{\sigma(1-v)}{E} \quad \text{[C2]}$$

φ, E and v are respectively the spherical strain, young's modulus of the sphere and poisson's ratio. The change in radius of this sphere is then given as,

$$r = r^0(1+\varphi) \quad \text{[C3]}$$

This gives the volume of the sphere as,

$$V = \frac{4}{3}\pi r^3 = \frac{4}{3}\pi[r^0(1+\varphi)]^3 = V^0(1+\varphi)^3 \quad \text{[C4]}$$

The compressibility as defined in Eq. [9], is then given as,

$$C_C = -\frac{1}{V}\frac{dV}{d\sigma} = -\frac{1}{P}\frac{(V-V^0)}{V^0} \quad \text{[C5]}$$

APPENDIX D: Code

```
clc
clear all
global V0 Ri0 gx s n F abs0 I dv v0 Omega Ce Cc_E1 Cc_E2 Cc_S
%------------------------constants that are estimated-----------------
------
V0    = 10e-6; % Initial Electrode Volume
Ri0   = 0.1;   % initial resistance
gx    = 0.334; % fraction of the volume, comprising the x-dimension
%------------------------Material constants---------------------------
------
s     = -1;
n     = 3.75;
F     = 96500;
abs0  = 0.5;   % initial porosity
v0    = 12.0590e-6; % Molar volume
dv    = 12.0590e-6; % 100% change in volume
%----------------------Constants that need to be measured------------
------
Ce    = 10.000e-009;% Compressibility of the electrode
Cc_E1 = 1.000e-009; % Compressibility of Aluminum casing (Al)
Cc_E2 = Cc_E1*5;    % Compressibility of Epoxy Resin casing (ER)
Cc_S  = 1.2500e-018;% Compressibility of stiff casing

theta1 = Ce/Cc_E1;  % Relative compressibility of Aluminum
theta2 = Ce/Cc_E2;  % Relative compressibility of Epoxy Resin
I      = 1;         % Applied Current

Qmax  = n*F*V0*(1-abs0)/(-s*dv);  % maximum charge in the electrode
tmax  = round(Qmax/I)            % time needed to discharge/recharge

tic;
[si_g_1,abs_i_g_1]     = ode45(@dabs_g1,[0 5e10],abs0);  % Al
[si_g_2,abs_i_g_2]     = ode45(@dabs_g2,[0 5e10],abs0);  % ER
[si_g0,abs_i_g0]   = ode45(@dabs_g0,[0 5e10],abs0);      % Stiff casing

%            Initial values
stress_g_1(1,1) = 0;
stress_g_2(1,1) = 0;
stress_g0(1,1)  = 0;
abs_g_1(1,1)    = abs0;
abs_g_2(1,1)    = abs0;
abs_g0(1,1)     = abs0;
%%%%%%%%%%%%%%%%%%%%%%     equilibrium  %%%%%%%%%%%%%%%%%%%%%%%%%%%%%%%%
```

```
Q_eq   = [1:1:tmax]'.*I;
SOC_eq = Q_eq./Qmax;
dEeq   = -0.059.*log(SOC_eq./(1-SOC_eq));
dERED  = dEeq - I*Ri0;
% % % %%%%%%%%%%%%%%%%%%%%%%%%%%%%%% Theta = 0 %%%%%%%%%%%%%%%%%%%%%%%%%%
stress_g1(1:1:tmax,1) = 0;
phi_g1                = exp(-Ce.*stress_g1) - 1 +
                          (dv/v0).*([1:1:tmax]'./tmax);
V_g1                  = V0.*(1 + phi_g1);
abs_g1(1:1:tmax,1)    = abs0;
Ri_g1                 = Ri0.*((V_g1./V0).^(2*gx-1));
Q_g1                  = [1:1:tmax]'.*I;
SOC_g1                = Q_g1./Qmax;
dE_g1_eq              = -0.059.*log(SOC_g1./(1-SOC_g1));
dE_g1                 = dE_g1_eq - I.*Ri_g1;

%%%%%%%%%%%%%%%%%%%%%%%%% Variable Theta %%%%%%%%%%%%%%%%%%%%%%%%%%%%%%%%

%%%%%%
for i = 2:1:tmax
    handle_g_1 = @(x)(exp(-Ce*x) - 1 + (dv/v0)*(i/tmax) - x*Cc_E1);
    stress_g_1(i,1) = fzero(handle_g_1,0);
    abs_g_1(i,1) = interp1(si_g_1,abs_i_g_1,stress_g_1(i,1));
end
phi_g_1 = exp(-Ce.*stress_g_1) - 1 + (dv/v0).*([1:1:tmax]'./tmax);
V_g_1   = V0.*(1 + phi_g_1);
Ri_g_1  = Ri0.*((V_g_1./V0).^(2*gx-1))./((abs_g_1./abs0).^1.5);
Q_g_1   = [1:1:tmax]'.*I;
SOC_g_1 = Q_g_1./Qmax;
dE_g_1_eq = -0.059.*log(SOC_g_1./(1-SOC_g_1));
dE_g_1    = dE_g_1_eq - I.*Ri_g_1;
%%%%%% ER
for i = 2:1:tmax
    handle_g_2 = @(x)(exp(-Ce*x) - 1 + (dv/v0)*(i/tmax) - x*Cc_E2);
    stress_g_2(i,1) = fzero(handle_g_2,0);
    abs_g_2(i,1) = interp1(si_g_2,abs_i_g_2,stress_g_2(i,1));
end
phi_g_2 = exp(-Ce.*stress_g_2) - 1 + (dv/v0).*([1:1:tmax]'./tmax);
V_g_2   = V0.*(1 + phi_g_2);
Ri_g_2  = Ri0.*((V_g_2./V0).^(2*gx-1))./((abs_g_2./abs0).^1.5);
Q_g_2   = [1:1:tmax]'.*I;
SOC_g_2 = Q_g_2./Qmax;
dE_g_2_eq = -0.059.*log(SOC_g_2./(1-SOC_g_2));
dE_g_2    = dE_g_2_eq - I.*Ri_g_2;

%%%%%%%%%%%%%%%%%%%%%%%%%%%% Theta = inf %%%%%%%%%%%%%%%%%%%%%%%%%%%%%%%%
for i = 2:1:tmax
    handle_g0 = @(x)(exp(-Ce*x) - 1 + (dv/v0)*(i/tmax));
    stress_g0(i,1) = fzero(handle_g0,0);
    abs_g0(i,1) = interp1(si_g0,abs_i_g0,stress_g0(i,1));
end
phi_g0(1:1:tmax,1) = 0;
V_g0(1:1:tmax,1) = V0;
Ri_g0            = Ri0./((abs_g0./abs0).^1.5);
Q_g0             = [1:1:tmax]'.*I;
SOC_g0           = Q_g0./Qmax;
```

```
dE_g0_eq          = -0.059.*log(SOC_g0./(1-SOC_g0));
dE_g0             = dE_g0_eq - I.*Ri_g0;


plot(SOC_g0(1:1:tmax),phi_g0(1:1:tmax,1),SOC_g1(1:1:tmax),phi_g1(1:1:tm
ax,1),
'g',SOC_g_1(1:1:tmax),phi_g_1(1:1:tmax,1),'k',SOC_g_2(1:1:tmax),phi_g_2
(1:1:tmax,1),'c')
xlabel('SOC');
ylabel('Electrode strain, \phi'); pause

plot(SOC_g0(1:1:tmax),abs_g0(1:1:tmax,1),SOC_g1(1:1:tmax),abs_g1(1:1:tm
ax,1),'g',SOC_g_1(1:1:tmax),abs_g_1(1:1:tmax,1),'k',SOC_g_2(1:1:tmax),a
bs_g_2(1:1:tmax,1),'c')
xlabel('SOC');
ylabel('Porosity, \epsilon'); pause

plot(SOC_g0(1:1:tmax),V_g0(1:1:tmax,1),SOC_g1(1:1:tmax),V_g1(1:1:tmax,1
),'g',SOC_g_1(1:1:tmax),V_g_1(1:1:tmax,1),'k',SOC_g_2(1:1:tmax),V_g_2(1
:1:tmax,1),'c')
xlabel('SOC');
ylabel('Volume'); pause

plot(SOC_g0(1:1:tmax),stress_g0(1:1:tmax,1)./1e6,SOC_g1(1:1:tmax),stres
s_g1(1:1:tmax,1)./1e6,'g',SOC_g_1(1:1:tmax),stress_g_1(1:1:tmax,1)./1e6
,'k',SOC_g_2(1:1:tmax),stress_g_2(1:1:tmax,1)./1e6,'c')
xlabel('SOC');
ylabel('Hydrostatic Stress, \sigma (MPa)'); pause

plot(SOC_g0(1:1:tmax-3),Ri_g0(1:1:tmax-
3,1)./Ri0,SOC_g1(1:1:tmax,1),Ri_g1(1:1:tmax,1)./Ri0,'g',SOC_g_1(1:1:tma
x),Ri_g_1(1:1:tmax,1)./Ri0,'k',SOC_g_2(1:1:tmax),Ri_g_2(1:1:tmax,1)./Ri
0,'c')
axis([0 1 1 6]);
xlabel('SOC');
ylabel('ioninc res'); pause

plot(SOC_eq(2:1:tmax),dEeq(2:1:tmax,1),SOC_eq(2:1:tmax),dERED(2:1:tmax,
1),'r',SOC_g0(1:1:tmax),dE_g0(1:1:tmax,1),'c',SOC_g1(2:1:tmax),dE_g1(2:
1:tmax,1),'g',SOC_g_1(1:1:tmax),dE_g_1(1:1:tmax,1),'k',SOC_g_2(1:1:tmax
),dE_g_2(1:1:tmax,1),'c')
axis([0 1 -0.4 0.4]);
xlabel('SOC');
ylabel('Nerst Potential, E(V)'); pause


%%%%%%%%%%%%%%%%%%%%%%%%%%% Swelling Coefficient, %%%%%%%%%%%%%%%%%%%%%
g_g0    = (1-abs_g0)./((1-abs0)*(v0/dv)*(1+inf.*exp(-Ce.*stress_g0)) -
(1-
           abs_g1).*stress_g0.*0);          % Theta = inf

g_g_1   = (1-abs_g_1)./((1-abs0)*(v0/dv)*(1+theta1.*exp(-
Ce.*stress_g_1)) -
          (1-abs_g_1).*stress_g_1.*Cc_E1);    % Al
```

```
g_k_g_2 = (1-abs_g_2)./((1-abs0)*(v0/dv)*(1+theta2.*exp(-
Ce.*stress_g_2)) -
          (1-abs_g_2).*stress_g_2.*Cc_E2); % ER

g_k_g1  = (1-abs_g1)./((1-abs0)*(v0/dv)*(1+0.*exp(-Ce.*0)) - (1-
           abs_g1).*0.*inf);                % Theta = 0


toc;
%%%%%%%%%%%%%%%%%%%%%%%% FUNCTIONS %%%%%%%%%%%%%%%%%%%%%%%%%%%%%%%%%%%%

% Al
function kk = dabs_g1(si_g_1,abs_i_g_1)
global V0 Ri0 gx s n F abs0 I dv v0 Omega Ce Cc_E1 Cc_E2 Cc_S
kk =-(1-abs0)*(Cc_E1 + Ce*exp(-Ce*si_g_1))/(1+si_g_1*Cc_E1) + (1-
      abs_i_g_1)*Cc_E1;

% ER
function kk = dabs_g2(si_g_2,abs_i_g_2)
global V0 Ri0 gx s n F abs0 I dv v0 Omega Ce Cc_E1 Cc_E2 Cc_S
kk =-(1-abs0)*(Cc_E2 + Ce*exp(-Ce*si_g_2))/(1+si_g_2*Cc_E2) + (1-
      abs_i_g_2)*Cc_E2;

% Stiff casing
function kk = dabs_g0(si_g0,abs_i_g0)
global V0 Ri0 gx s n F abs0 I dv v0 Omega Ce Cc_E1 Cc_E2 Cc_S
kk = -(1-abs0)*(Cc_S + Ce*exp(-Ce*si_g0))/(1+si_g0*Cc_S) + (1-
       abs_i_g0)*Cc_S;
```

APPENDIX E: Battery Model

If a battery setup is considered, there is an electrolyte membrane/separator, sandwiched between two porous electrodes. Assuming that the volume change in mixing is negligible, the material balance over the solid phase (active material + reaction product) governs the volume change in both electrodes as,

$$\frac{\partial(1-\varepsilon_i)}{\partial t} + \boldsymbol{\nabla}\cdot[(1-\varepsilon_i)\boldsymbol{u_i}] = -\frac{s_i\,\Delta\widehat{V}_i}{n_i\mathcal{F}} j_i \,, here\ i = P, N \qquad \text{[E1]}$$

The subscript, P and N indicate the positive and the negative electrode. Here, the porosity, the local electrode velocity and the local volumetric current density, for both porous electrodes are assumed to be a continuous function of location. The local electrode velocity is a smooth function thus its gradient can further be expressed as rate change of the volumetric strain,

$$\boldsymbol{\nabla}\cdot\boldsymbol{u} = \frac{\partial}{\partial x_i}\frac{\partial}{\partial t}\boldsymbol{u_i} = \frac{\partial}{\partial t}\frac{\partial}{\partial x_i}\boldsymbol{u_i} = \frac{\partial}{\partial t}\boldsymbol{u_{i,i}} = \frac{\partial}{\partial t}\left[\frac{1}{2}\left(\boldsymbol{u_{i,i}} + \boldsymbol{u_{i,i}}\right)\right] = \frac{\partial\varphi}{\partial t} \qquad \text{[E2]}$$

Using Eq. [E2] in Eq. [E1] gives the governing relationship between the porosity and the volumetric strain of the electrode during intercalation.

$$\frac{\partial(1-\varepsilon_i)}{\partial t} + \boldsymbol{u_i}\cdot\boldsymbol{\nabla}(1-\varepsilon_i) + (1-\varepsilon_i)\frac{\partial\varphi_i}{\partial t} = -\frac{s_i\,\Delta\widehat{V}_i}{n_i\mathcal{F}} j_i \,, here\ i = P, N \qquad \text{[E3]}$$

Assuming uniform reaction current (I) and uniform porosity distribution (i.e. ε_i is uniform), Eq. [E3] can be simplified as

$$\frac{\partial}{\partial t}(1-\varepsilon_i)+(1-\varepsilon_i)\frac{\partial \varphi_i}{\partial t}=-\frac{s_i\,\Delta\hat{V}_i}{n_i\mathcal{F}}\frac{I}{V_i}, here\ i=P,N \quad \text{[E4]}$$

Furthermore the current volume of each electrode is defined as

$$V_P = V_P^0(1+\varphi^P) \quad \text{[E5a]}$$

$$V_C = V_C^0(1+\varphi^N) \quad \text{[E5b]}$$

Substitution of Eq. [E5] in Eq. [E4], results in

$$(1+\varphi_P)\frac{\partial}{\partial t}(1-\varepsilon_P)+(1-\varepsilon_P)(1+\varphi_P)\frac{\partial \varphi_P}{\partial t}=-\frac{s_P\,\Delta\hat{V}_P}{n_P\mathcal{F}}\frac{I}{V_P^0} \quad \text{[E6a]}$$

$$(1+\varphi_N)\frac{\partial}{\partial t}(1-\varepsilon_N)+(1-\varepsilon_N)(1+\varphi_N)\frac{\partial \varphi_N}{\partial t}=-\frac{s_N\,\Delta\hat{V}_N}{n_N\mathcal{F}}\frac{I}{V_N^0} \quad \text{[E6a]}$$

The volumetric strain of the electrode, analogous to thermal-mechanical strain [33] is made up of two parts. The first is the mechanical strain, 'φ_M' (caused by the mechanical stress) and the second is the intercalation strain, 'φ_I' (caused by the addition of intercalate into the solid phase). Mathematically the volumetric electrode strain for both electrodes can be expressed as

$$\varphi_P = \varphi_{M,P} + \varphi_{I,P} \quad \text{[E7a]}$$

$$\varphi_N = \varphi_{M,N} + \varphi_{I,N} \quad \text{[E7b]}$$

Considering uniform expansion everywhere in the electrode, i.e. assuming that there are no transport limitations within the active material of the electrode, and also since the volume of the porous material can be measured before and after intercalation. The chemical strain of each electrode can be defined similar to Obrovac et al. [13] as,

$$\varphi_{I,P} = \left[\frac{\Delta \hat{V}_P}{\hat{V}_P{}^0}\right] x \qquad \text{[E8a]}$$

$$\varphi_{I,N} = \left[\frac{\Delta \hat{V}_N}{\hat{V}_N{}^0}\right] x \qquad \text{[E8b]}$$

Similar to the previous model developed, for both porous electrodes treated as a smeared continuum made up of fractions of solid phases and pores, the compressibility's of each electrode analogous to the treatment in rock mechanics [41, 42] is defined as,

$$C_{E,P} = -\frac{1}{V_P}\frac{dV_P}{d\sigma} \qquad \text{[E9a]}$$

$$C_{E,N} = -\frac{1}{V_N}\frac{dV_N}{d\sigma} \qquad \text{[E9b]}$$

Differentiating the of mechanical volume and noting that mechanical stress (σ) only affects the volume change due to mechanical strain, Eq. [E9] can be re-written as

$$\frac{dV_{P,M}}{V_{P,M}} = \frac{d(1+\varphi_{M,P})}{(1+\varphi_{M,P})} \qquad \text{[E10a]}$$

$$\frac{dV_{N,M}}{V_{N,M}} = \frac{d(1+\varphi_{M,N})}{(1+\varphi_{M,N})} \qquad \text{[E10b]}$$

Substitution of Eq. [E10] into Eq. [E9] and performing integration gives the mechanical strain of the electrode as

$$\varphi_{M,P} = exp(-C_E^P \sigma^P) - 1 \qquad \text{[E11a]}$$

$$\varphi_{M,N} = exp(-C_E^N \sigma^N) - 1 \qquad \text{[E11b]}$$

The total electrode strain is then defined by using Eq. [E7], Eq. [E8] and Eq. [E11] as,

$$\varphi^P = exp(-C_E^P \sigma^P) - 1 + \left[\frac{\Delta \hat{V}_P}{\hat{V}_P{}^0}\right] x \qquad \text{[E12a]}$$

$$\varphi^N = exp(-C_E^N \sigma^N) - 1 + \left[\frac{\Delta \hat{V}_N}{\hat{V}_N{}^0}\right] x \qquad \text{[E12b]}$$

Assuming a compliant separator, the hydrostatic pressure inside the battery is in equilibrium. This would mean that hydrostatic stress in the positive electrode equals that in the negative electrode.

$$\sigma^P = \sigma^N = \sigma \qquad \text{[E13]}$$

Using Eq. [E13], Eq. [E12 is re-written as,

$$\varphi^P = exp(-C_E^P \sigma) - 1 + \left[\frac{\Delta \hat{V}_P}{\hat{V}_P{}^0}\right] x \qquad \text{[E14a]}$$

$$\varphi^N = exp(-C_E^N \sigma) - 1 + \left[\frac{\Delta \hat{V}_N}{\hat{V}_N{}^0}\right] x \qquad \text{[E14b]}$$

Since, the total volume of the battery is the sum total of both the electrodes and the separator, it is given as

$$V = V_P + V_N + V_S \qquad \text{[E15]}$$

Here, the subscript S stands for separator and since the volume of the separator does change, using Eq. [5], Eq. [E15] is given as,

$$V = V^0(1 + \varphi) = V_P^0(1 + \varphi_P) + V_N^0(1 + \varphi_N) + V_S^0 \qquad \text{[E16]}$$

$$\varphi = \frac{V_P^0}{V^0}\varphi_P + \frac{V_N^0}{V^0}\varphi_N \qquad \text{[E17]}$$

Substituting, Eq. [E14] in Eq. [E17] gives,

$$\varphi = \frac{V_P^0}{V^0}\left[exp\left(-C_{P,E}\sigma\right) - 1 + \left[\frac{\Delta\widehat{V}_P}{\widehat{V}_P{}^0}\right]x\right] + \frac{V_N^0}{V^0}\left[exp\left(-C_{N,E}\sigma\right) - 1 + \left[\frac{\Delta\widehat{V}_N}{\widehat{V}_N{}^0}\right]x\right] \quad \text{[E18]}$$

Typically the porous electrodes are enclosed in a casing to hold the electrolyte, provide support to the electrodes and facilitate electrical contact. A casing restrains volume expansion of the electrodes and hence induces mechanical stresses within the electrode. It is assumed that the casing undergoes small to medium deformation when there is large deformation in the electrode. Due to this the total electrode strain (battery strain) is given as

$$\varphi = \sigma C_C \quad \text{[E19]}$$

The porosity-stress relationship defined in the earlier model is still valid, but now there is a need for this relationship to be defined for both electrodes and is given as,

$$\frac{d}{d\sigma}(1-\varepsilon_P) + (1-\varepsilon_P)C_c = \frac{C_c\left(1-\varepsilon_P^0\right)}{[1+\sigma C_c]}\left[1 + \theta_P exp\left(-C_{E,P}\sigma\right)\right] \quad \text{[E20a]}$$

$$\frac{d}{d\sigma}(1-\varepsilon_N) + (1-\varepsilon_N)C_c = \frac{C_c\left(1-\varepsilon_N^0\right)}{[1+\sigma C_c]}\left[1 + \theta_N exp\left(-C_{E,N}\sigma\right)\right] \quad \text{[E20b]}$$

Performing integration on Eq. [E20] gives the porosity of both the electrodes as a function of stress, for integration look at APPENDIX: A

$$\varepsilon_P(\sigma) = 1 - (1-\varepsilon_P^0)e^{(-1-\sigma C_c)}\mathrm{Ei}(-1-\sigma C_c) - \theta_P(1-\varepsilon_P^0)\, e^{(-1-\theta_P-\sigma C_c)}\mathrm{Ei}(-1+\theta_P + (-1+\theta_P)\sigma C_c) + c_P e^{(-\sigma C_c)} \quad \text{[E21a]}$$

$$\varepsilon_N(\sigma) = 1 - (1-\varepsilon_N^0)e^{(-1-\sigma C_c)}\mathrm{Ei}(-1-\sigma C_c) - \theta_N(1-\varepsilon_N^0)\, e^{(-1-\theta_N-\sigma C_c)}\mathrm{Ei}(-1+\theta_N + (-1+\theta_N)\sigma C_c) + c_N e^{(-\sigma C_c)} \quad \text{[E21b]}$$

The discussion in Gomadam et al.[32] defined a constant parameter called as the swelling coefficient which determines the fraction of volume expansion that goes into the change in porosity and the fraction that goes into the change in dimensions of the electrode (volume of the electrode) and is defined as

$$g = \frac{\frac{d\,lnV}{d\,ln(1-\varepsilon)}}{1+\frac{d\,lnV}{d\,ln(1-\varepsilon)}} \qquad \text{[E22]}$$

Here, the swelling coefficient needs to be defined for both the electrodes as it is not held constant as in Gomadam et al.[32] but is calculated similarly during intercalation (for derivation look at APPENDIX: B). The analytical solution for the swelling coefficient in both the electrodes is then given as,

$$g_P = \frac{(1-\varepsilon_P)}{(1-\varepsilon_P^0)[1+\theta_P exp(-C_{P,E}\sigma)\,]-(1-\varepsilon_P)C_C\sigma} \qquad \text{[E23a]}$$

$$g_N = \frac{(1-\varepsilon_N)}{(1-\varepsilon_N^0)[1+\theta_N exp(-C_{N,E}\sigma)\,]-(1-\varepsilon_N)C_C\sigma} \qquad \text{[E23b]}$$

During the expansion of the porous electrodes, there is change in dimensions of the electrode, which may or may not be uniform. To calculate the change in dimensions of the electrode, it is then necessary to calculate the individual components of the velocity. Substituting Eq. [16] and using Eq. [17] in Eq. [2] we can write

$$\boldsymbol{\nabla}\cdot\boldsymbol{u_i} = \frac{d\varphi_i}{dt} = C_c\frac{\frac{d\varphi_I}{dt}}{C_c-\frac{d\varphi_M}{d\sigma}}, here\ i = P, N \qquad \text{[E24]}$$

When the local electrode velocity is expressed as individual components, Eq. [E24] is re-written as

$$\frac{d\boldsymbol{u}_{i,x}}{dx}+\frac{d\boldsymbol{u}_{i,y}}{dy}+\frac{d\boldsymbol{u}_{i,z}}{dz}=\frac{d\varphi_i}{dt}=\left[\frac{\Delta\hat{V}}{\hat{V}^0}\right]\frac{dx_i}{dt}\left(\frac{1}{1+\theta exp(-C_E\sigma)}\right), here\ i=P,N \quad [E25]$$

To obtain local electrode velocities in each direction, Eq. [E25] can be spilt by introducing splitting parameters $g_{i,x}, g_{i,y}$ and $g_{i,z}$ to give,

$$\frac{d\boldsymbol{u}_{i,x}}{dx}=g_{i,x}\left[\left[\frac{\Delta\hat{V}}{\hat{V}^0}\right]\frac{dx_i}{dt}\left(\frac{1}{1+\theta exp(-C_E\sigma)}\right)\right], here\ i=P,N \quad [E26a]$$

$$\frac{d\boldsymbol{u}_{i,y}}{dx}=g_{i,y}\left[\left[\frac{\Delta\hat{V}}{\hat{V}^0}\right]\frac{dx_i}{dt}\left(\frac{1}{1+\theta exp(-C_E\sigma)}\right)\right], here\ i=P,N \quad [E26b]$$

$$\frac{d\boldsymbol{u}_{i,z}}{dx}=g_{i,z}\left[\left[\frac{\Delta\hat{V}}{\hat{V}^0}\right]\frac{dx_i}{dt}\left(\frac{1}{1+\theta exp(-C_E\sigma)}\right)\right], here\ i=P,N \quad [E26c]$$

Here the splitting parameters g_x, g_y and g_z, determine how much of the electrode's dimensional change is due to the change in the dimensions in x, y and z direction. They can be defined as, similar to Gomadam et al. [40]

$$g_{i,x}=\frac{d\varphi_{i,x}}{d\varphi_i}, here\ i=P,N \quad [E27a]$$

$$g_{i,y}=\frac{d\varphi_{i,y}}{d\varphi_i}, here\ i=P,N \quad [E27b]$$

$$g_{i,z}=\frac{d\varphi_{i,z}}{d\varphi_i}, here\ i=P,N \quad [E27c]$$

The change in ionic and electronic resistance of the porous electrode due to volume change during operation, is given by [32], but they need to be defined for both electrodes as,

$$\frac{R_{i,P}}{R_{i,N}^0}=\frac{L_{l,P}/L_{l,P}^0}{\left(A_P/A_P^0\right)\left(\varepsilon_P/\varepsilon_P^0\right)^{1.5}}, l=x,y,z \quad [E28a]$$

$$\frac{R_{i,N}}{R_{i,N}^0}=\frac{L_{l,N}/L_{l,N}^0}{\left(A_N/A_N^0\right)\left(\varepsilon_N/\varepsilon_N^0\right)^{1.5}}, l=x,y,z \quad [E28b]$$

$$\frac{R_{e,P}}{R_{e,P}^0}=\frac{L_{l,P}/L_{l,P}^0}{\left(A_P/A_P^0\right)\left(\varepsilon_{e,P}/{\varepsilon_{e,P}}^0\right)^{1.5}}, l=x,y,z \quad [E29a]$$

$$\frac{R_{e,N}}{R_{e,N}^0} = \frac{L_{l,N}/L_{l,N}^0}{(A_N/A_N^0)(\varepsilon_{e,N}/{\varepsilon_{e,N}}^0)^{1.5}}, l = x, y, z \quad \text{[E29a]}$$

The dimensions of both electrodes are defined as,

$$\frac{L_{i,P}}{L_{i,P}^0} = \left(\frac{V_P}{V_P^0}\right)^{g_l}, l = x, y, z \quad \text{[E30a]}$$

$$\frac{L_{i,N}}{L_{i,N}^0} = \left(\frac{V_N}{V_N^0}\right)^{g_l}, l = x, y, z \quad \text{[E30b]}$$

$$\frac{A_P}{A_P^0} = \left(\frac{V_P}{V_P^0}\right)^{1-g_l}, l = x, y, z \quad \text{[E31a]}$$

$$\frac{A_N}{A_N^0} = \left(\frac{V_N}{V_N^0}\right)^{1-g_l}, l = x, y, z \quad \text{[E31b]}$$

Here, $g_{i,x}, g_{i,y}$and $g_{i,z}$ determines the change in dimensions of the electrode, in x, y and z directions due to electrode volume change as defined by Gomadam et al. 32 and Eq. [E30] determines splitting parameters for both electrodes. For the purpose of this work these are considered constant. Individual electrode potentials can be calculated as,

$$E_P = E_P^0 - 0.059\ln\left(\frac{x}{1-x}\right) \quad \text{[E32a]}$$

$$E_N = E_N^0 - 0.059\ln\left(\frac{x}{1-x}\right) \quad \text{[E32b]}$$

The cell potential is then defined as,

$$E_{Cell} = E_P - E_N \quad \text{[E32c]}$$